2009

Inestigation of the energy variation on a TomoTherapy HI-Art II using an aluminum stepwedge

Todd Racine
Louisiana State University and Agricultural and Mechanical College

INVESTIGATION OF THE ENERGY VARIATION ON A TOMOTHERAPY HI-ART II USING AN ALUMINUM STEPWEDGE

A Thesis

Submitted to the Graduate Faculty of the
Louisiana State University and
Agricultural and Mechanical College
in partial fulfillment of the
requirements for the Degree of
Master of Science

in

The Department of Physics & Astronomy

by
Todd Michael Racine
B.S. Ball State University, May 2006
December 2009

Acknowledgements

I thank the members of my advisory committee for all of their assistance and guidance; Dr. John Gibbons for his leadership and encouragement throughout the project: Dr. Kenneth Hogstrom for the opportunity to come to LSU as well as his ideas and perspective; Dr. Jonas Fontenot for his input and assistance; Dr. Monica Moldovan for her willingness to lend a hand when I was unable to take a reading; and Dr. Jim Matthews for encouragement and oversight from the department. I thank the entire staff at Mary Bird Perkins Cancer Center, for the use of their equipment as well showing me how to operate it properly.

I thank all of the therapists, dosimetrists, doctors, physicists, and those who aided in my education throughout the program. Also, thanks to all of those who helped teach the classes and gave us their time. Thanks to the medical physics support staff who helped with anything I needed administratively.

I thank my parents, Randy and Nancy Racine, for all of their support. Thanks to TomoTherapy, Inc. for making this work possible. I would also like to thank the medical physics students for their needed distraction.

Table of Contents

List of Tables

List of Figures

Abstract

Purpose: To determine the sensitivity of a topographic stepwedge procedure to energy variations in a helical tomotherapy system.

Method and Materials: Topographic procedures were followed using an aluminum stepwedge suspended in air on the end of the couch for a TomoTherapy HI-Art II system. Exit detector data from these procedures, collected and processed using TomoTherapy quality assurance (TQA) software were used to determine the effective beam energy. Energy sensitivity tests of the technique were made by varying the injector current. Topographic procedures were run daily over the lifetime of an x-ray target. Additionally, water phantom scanning data (lateral profiles and percent depth dose) were measured monthly over the same time period.

Results: The attenuation data from the stepwedge demonstrated a smooth decrease in effective energy with time over the life of the target. The energy difference showed dramatic spikes in trending due to target changes and injector current adjustments. Monthly lateral and depth-dose profiles showed variations due to an energy change but not while a target was simultaneously degrading. Analysis of the data show that the stepwedge procedure is capable of detecting a change in the effective energy of greater than 2%.

Conclusion: The stepwedge topographic procedure provides a good method to monitor the energy difference over time and may be used to help diagnose impending target failures.

Chapter 1. Introduction

I. Background and Significance

A. Introduction to TomoTherapy HI-ART

Tomotherapy, literally meaning slice therapy, is an innovative approach to radiation therapy that has recently been developed and implemented into the clinic. The TomoTherapy HI-ART combines intensity modulated radiation therapy (IMRT) capabilities with those of megavoltage computed tomography (CT) by mounting a linear accelerator (linac) onto a CT ring gantry.

IMRT refers to a radiation therapy technique in which a non-uniform fluence is delivered to the patient from multiple positions of the treatment beam, which together optimize the composite dose distribution (Khan 2003). Although a non-uniform fluence can be delivered in a number of ways (wedges, dynamic jaws, transmission blocks, or compensating filters), the term IMRT usually refers to delivery through the use of compensating filters or multileaf collimators (MLC). MLCs are positioned in the path of the beam during treatment for various lengths of time changing the intensity map and conforming to the patient. In order to optimize the dose to the patient, an "inverse planning" method is used. The treatment goals and criteria are set by the planner and the optimal fluence profiles used to achieve these goals are calculated by the planning computer system.

IMRT delivery may be performed by either gantry static or gantry dynamic methods, defined by whether or not the radiation source is moving during radiation delivery (Purdy 2001). Gantry static IMRT can be accomplished through the use of compensators, segmental MLC (SMLC) or step and shoot IMRT, and dynamic MLC (DMLC) or sliding window IMRT. Compensators can be easily manufactured (e.g.

.decimal, Inc.) and have varying attenuation and fluence resolution depending on the material used for the compensator (Chang, Cullip et al. 2004). SMLC-IMRT is defined as treatment delivery when the collimator shape is constant during irradiation and changes between irradiations (Siochi 1999); (Bortfeld, Kahler et al. 1994). DMLC-IMRT is defined by treatment delivery when the collimator shape changes during irradiation (LoSasso, Chui et al. 1998).

Gantry dynamic IMRT can be accomplished through serial or helical tomotherapy, intensity modulated arc therapy (IMAT); (Yu 1997), or volumetric modulated arc therapy (VMAT); (Otto 2008) accomplished using Varian's RapidArc (Varian Medical Systems, Palo Alto, CA) and Elekta's Volumetric Modulated Arc Therapy (VMAT); (Elekta, Stockholm, Sweden).

In serial tomotherapy, the dose distributions are delivered slice by slice with the patient sequentially translated through the gantry between slice deliveries (Purdy and Starkschall 1999). The first serial tomotherapy device developed was the Peacock system by the NOMOS corporation (Best Nomos, Pittsburgh, PA); (Grant 1999). In this device, a special collimating system called the MIMic is used, also developed by the NOMOS corporation. The MIMic is a binary MLC which houses 40 leaves each of which project to 1 x 1 cm^2 at isocenter. It fits in the accessory tray holder on a linac and is controlled by a computer used at the operating station. This computer receives and monitors information such as gantry speed, gantry position, and leaf position as a function of gantry angle. During treatment, the gantry will rotate in an arc, wait for the table to increment a precise distance, and then repeat the process. Therefore, the position of the patient is of utmost importance in order to avoid hotspots or coldspots (Low, Mutic et al. 1999).

In helical tomotherapy, the dose distributions are delivered slice by slice with the patient translated through the machine bore continuously during gantry rotation (Mackie and Balog 1999). The first helical tomotherapy unit was the HI-ART system, developed by TomoTherapy, Inc. (TomoTherapy, Madison, WI). In the HI-ART system, a linac rotates using a slip-ring gantry around a fixed isocenter located 85 cm from the source. A diagram of the current TomoTherapy unit, HI-ART II, is shown in Figure 1. During treatment, the couch translates through the bore of the machine while the gantry rotates resulting in a helical delivery (Mackie and Olivera 2003); (Dyk 2005), shown in Figure 2.

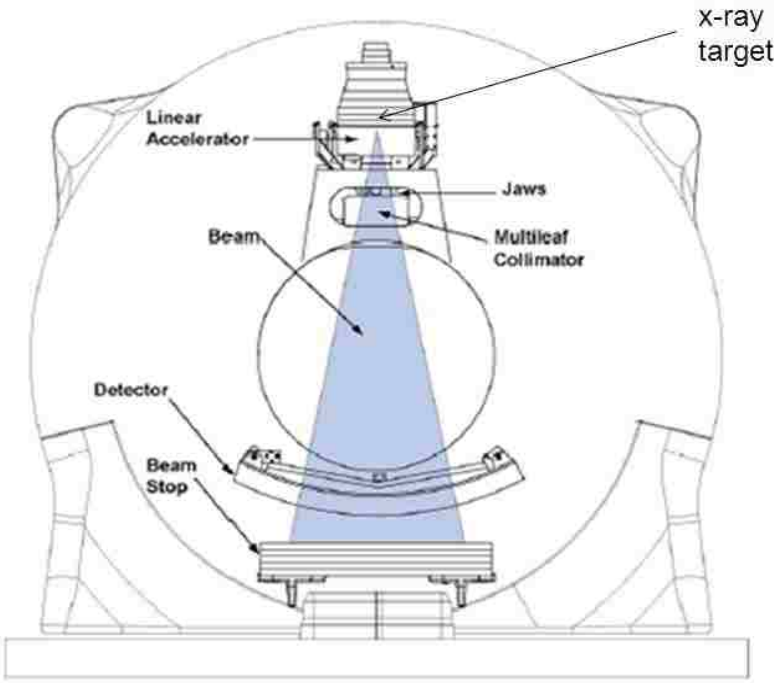

Figure 1. Diagram of TomoTherapy unit. In the TomoTherapy HI-ART II, the linear accelerator produces an electron beam which strikes an x-ray target producing the photon beam. The beam is then collimated into a fan beam, shown in blue, and upon exiting the patient, strikes an array of detectors (TomoTherapy 2007).

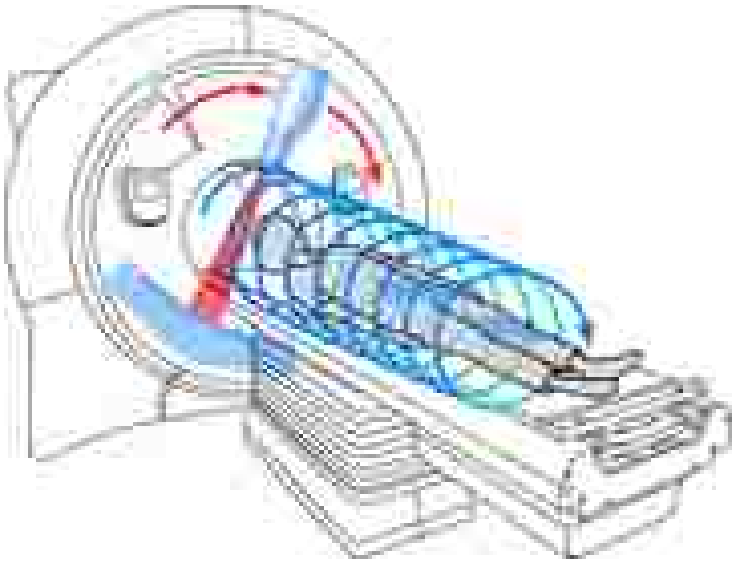

Figure 2. Illustration of helical delivery. The treatment couch translates into the bore of the machine while the gantry is rotating simultaneously, resulting in a helical delivery (Tomotherapy 2008).

In the HI-ART II helical tomotherapy system, the produced field of radiation is a fan beam and in the longitudinal direction along isocentric axis is defined by two collimating jaws that can be adjusted to deliver a field width ranging from 0.6-5.0 cm defined at the isocenter. In the lateral direction, a 64-leaf binary MLC is used to define the field shape. A binary MLC is an MLC, that has leaves that can be either open (allow passing of the beam) or closed (blocking the beam). This is illustrated in Figure 3. Each leaf projects to a width of 6.25 mm at isocenter, which for 64 leaves allows for field lengths ranging from 0-40 cm.

In IMRT, very high dose gradient regions are often produced. It is therefore crucial to position the patient accurately. Conventional linacs can use orthogonal MV planar radiographs prior to treatment to set patient positioning. These “port films” allow for adjustment in setup through visualization of bony anatomy. This can be a flawed

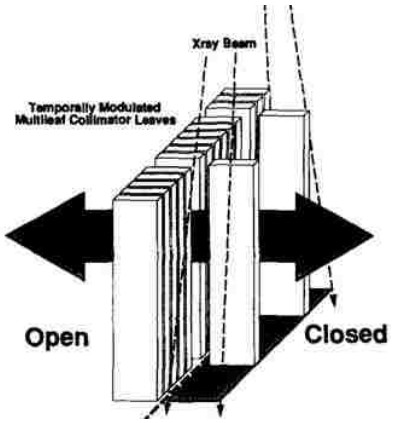

Figure 3**.** The binary MLC used for TomoTherapy (Mackie, Holmes et al. 1993). A leaf is either open (not blocking the beam) or closed (blocking the beam).

technique as soft tissue, such as the prostate, can move relative to the bony anatomy (Graf, Wust et al. 2009). The TomoTherapy HI-ART II system utilizes a megavoltage CT (MVCT) prior to treatment in order to verify the location of the patient. The TomoTherapy unit takes pre-treatment MVCT patient images and compares them to the diagnostic pre-treatment planned kilovoltage CT (kVCT) and makes necessary setup adjustments. Although MVCT images have inferior tissue contrast compared with kVCT, MVCT has much better tissue contrast than planar MV port film (Mackie and Balog 1999).

The radiation source used for the MVCT, as well as for treatment, is the same in-line linac. The linac's incoming electron beam is incident on a tungsten target which produces bremsstrahlung x-rays with a spectrum of energies ranging up to the potential difference of the system. The system used in this study utilizes maximum photon energies of approximately 6 MeV for therapy and approximately 3.5 MeV for MVCT (Mackie and Olivera 2003). The linac rotates using a slip-ring gantry around a fixed isocenter located 85 cm from the source. Opposite from the linac is an array of

detectors used to acquire the MVCT (see Figure 1). The detectors are a xenon ion chamber array consisting of several independent channels. Raw data is recorded for each pulse at a rate of 300 pulses per second for the detector array and three transmission ion monitor chambers in the head of the linac. These data are temporarily stored for each procedure. The temporary data set is stored as a compressed data set in the patient database located on a data server. The MVCT is used prior to treatment to evaluate the position of the patient and provide information if re-positioning is necessary. Also, during treatment the detectors collect the signal through the patient which may be used to reconstruct the delivered dose to the patient (Kapatoes, Olivera et al. 2001).

B. TomoTherapy x-ray Target

The x-ray target is struck by a small (approximately 1-mm diameter) beam of electrons (Mackie and Olivera 2003). High energy x-rays, or photons, are generated through bremsstrahlung processes and undergo Compton scattering. Ideally this target (see Figure 4) would be made of a high atomic number (Z) material to maximize the probability of bremsstrahlung radiation. The x-ray target for TomoTherapy is made of tungsten (Z=74). In order to maximize bremsstrahlung production and minimize absorption of the produced photons, the thickness of the target should be slightly thicker (~10%) than the electron range for that energy. Over the lifetime of the target, the tungsten will thin resulting in fewer low energy photons being absorbed thus lowering the average energy or “softening” the beam. Beam softening can be seen as a decrease in the intensity in the beam profile at the lateral edges (Langen, Meeks et al. 2005). An example of a new and used target are shown in Figure 4a and Figure 4b. Because a high intensity source of electrons generates heat, the target is rotated while

the beam is on in order to spread out the area where the electrons strike the target. This is accomplished by a flowing water system that also acts to cool the target. Nonetheless, targets can degrade, or thin, due to the high dose rates produced by the accelerator and the long beam on times used for TomoTherapy (Staton, Langen et al. 2009). This degradation of the target will impact beam profiles and energy, although we currently do not take any changes in the target into account in the treatment planning software. The lifetime of a target varies, depending on the workload. For a typical patient load of 20 patients/day, its lifetime is approximately one year.

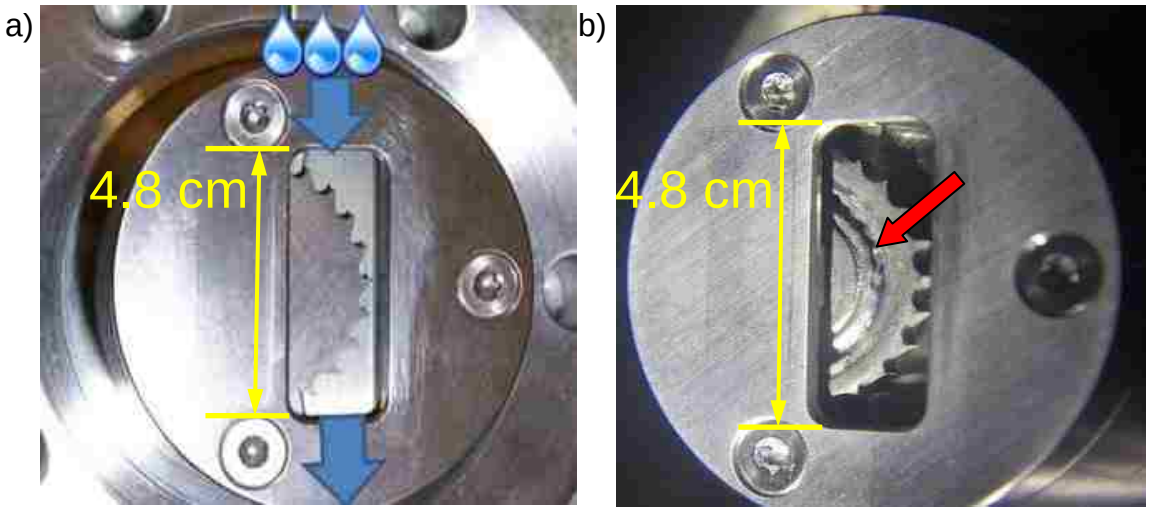

Figure 4. Photograph of two target assemblies used in our HI-ART II system. The target is a thin tungsten disk with teeth on the outer rim to aid in target rotation from water flowing across the assembly. Shown are a) a new, unused target illustrating water flow (blue arrows) and b) a used, degraded target with radial grooves (red arrow) worn in where the incident electron beam struck the disk.

C. Xenon Detector Array

The exit detector array on TomoTherapy consists of 738 xenon ion chambers. The signals from these chambers are used for pre-treatment MVCT, dose reconstruction from patient treatment, and quality assurance (QA) purposes. When used as a QA tool,

one common test performed is known as a rotational variation, or RotVar. In a RotVar, the exit detectors collect beam data from a procedure in which the collimating jaws are both completely open, the beam unattenuated, i.e. the table positioned out of the gantry, and the gantry constantly rotating. The resulting profile is known as a cone or lateral profile because of its similarity to a cone shape. An example cone profile is displayed in Figure 5a. The cone profile is essentially a lateral or transverse profile of the beam as seen from the detectors. The triangular or cone shape results from the fact that bremsstrahlung production (x-rays) from the target is forward peaked. The central dip in the profile results from the array of detectors being situated on an arc that is out of focus with the virtual x-ray source used for TomoTherapy. The arc that is housed was originally designed for use in a conventional CT scanner. A lateral profile taken from a scanning ion chamber in a water tank, as opposed to an out-of-focus array of detectors, is shown in Figure 5b for comparison. The exit detector array has a 1.1 m radius of curvature, while the source to detector distance is 1.42 m (Langen, Meeks et al. 2005). The individual ion chambers are separated by tungsten septa that intercept the beam at different angles due to the out of focus detector array. X-rays coming from the source vertically on the central axis will typically pass between the septa separating the xenon ionization detectors, whereas x-rays traveling off central axis will be oblique to the septal plates resulting in their striking one of the septa, producing electrons that will increase the ionization in that detector, see Figure 5c. Therefore, there is an increase in the number of counts lateral to the central axis of the beam resulting in the dip seen in the cone profile (Keller, Glass et al. 2002).

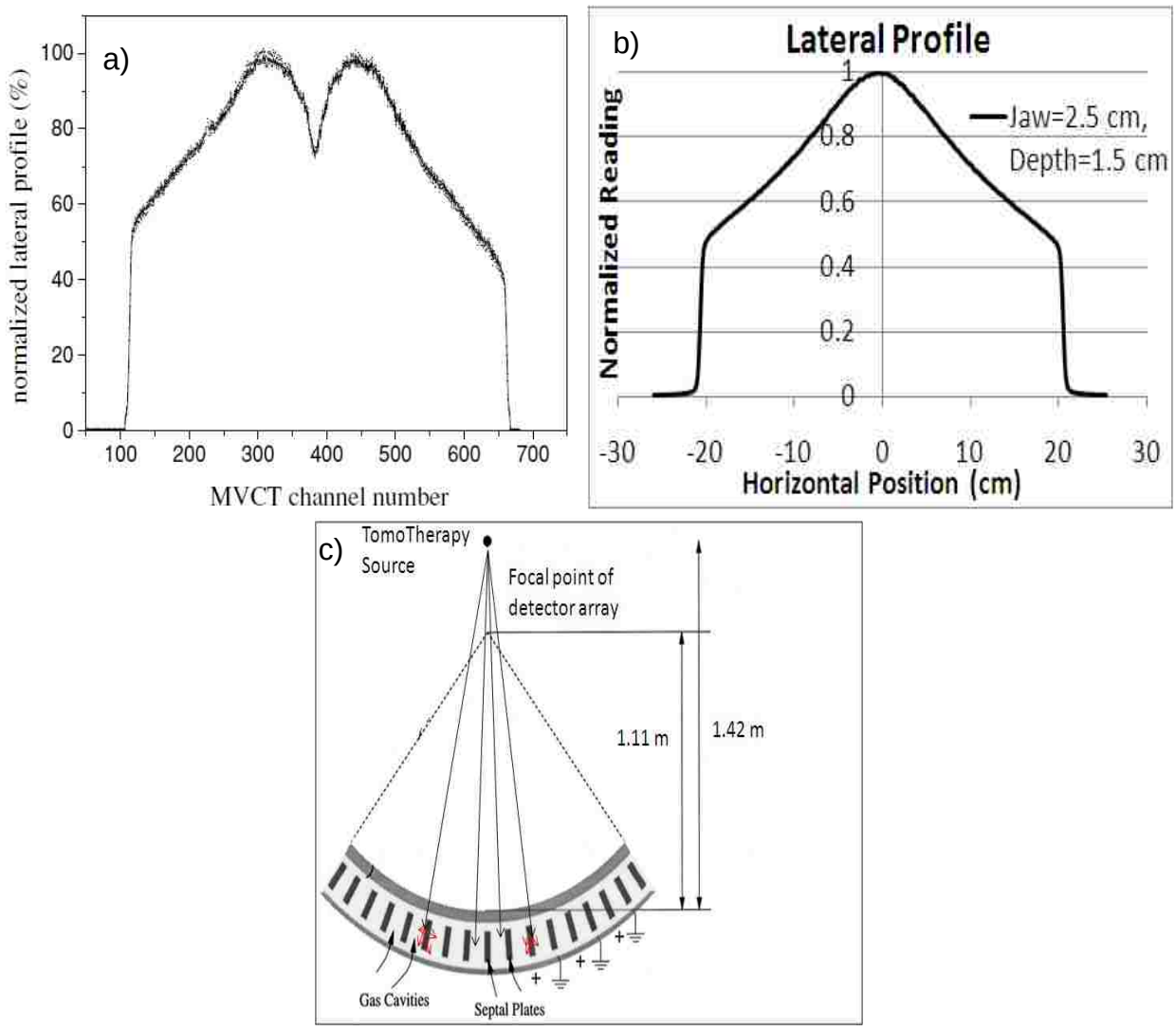

Figure 5. In-air cone or lateral profile. a) Lateral profile as seen from exit detector array (Fenwick, Tome et al. 2004), b) lateral profile from scanning ion chamber in water tank, and c) illustration showing detector array is out of focus with TomoTherapy source causing increased counts on either side of the central axis (Keller, Glass et al. 2002).

D. Monitoring of x-ray Target

Monitoring of the target can be done by looking for changes in beam characteristics over time. This has traditionally been accomplished by collecting cone profiles, both in air and water, over time. When collected in water, a tank is setup inside the bore of the treatment machine while data is collected using an ion chamber that scans across a

stationary beam in the transverse plane. This setup also allows depth-dose profiles to be collected, another useful method of analysis. When collected in air, data is processed using the on-board exit detector array from an unattenuated beam with a rotating gantry. In a degraded target, the shoulders of a lateral profile would sag, meaning the off-axis beam ratio would decrease (Staton, Langen et al. 2009). This results from beam softening over time. In-air cone profiles using the exit detectors are also used to monitor the target and are usually performed by a service engineer on a weekly basis.

As mentioned, a degraded target could result in the shoulders of a cone or lateral profile sagging. Another reason that the shoulders could sag would be a decrease in the energy of the beam as again photons would be absorbed prior to reaching off-axis areas. The two cannot be distinguished, however, using data gathered from an unattenuated beam. One possible way to remedy the sagging shoulders is to adjust the injector current setting of the machine. The injector current controls the amplitude of the electron gun pulse which determines the number of electrons entered into the beam (Karzmark, Nunan et al. 1993). When raised, the number of electrons in the beam increases, effectively reducing the energy of each individual electron, mainly due to space charge effects. Decreasing the injector current, and thus increasing the energy of each electron, results in less scatter and higher readings on the area of the lateral profile that would be affected by a change in energy of the beam, the shoulder or off-axis region.

i. Tomotherapy Quality Assurance (TQA)

In order to ensure that a TomoTherapy HI-ART II therapy machine is operating properly and generating the dose distributions expected, a quality assurance (QA) protocol

specific to TomoTherapy was developed (Fenwick, Tome et al. 2004). This protocol is an extension of the AAPM Task Group 40 (TG-40) report (Kutcher, Coia et al. 1994), the QA guidelines for conventional linear accelerators. The TG-40 report includes recommendations for linac features which are not applicable to TomoTherapy. Conventional linacs operate using a treatment couch that remains stationary during delivery. Traditionally, the gantry has also remained fixed, but newer technologies such as Varian's RapidArc and Elekta's VMAT utilize a rotating gantry during treatment. Some features of conventional linacs include a flattening filter, which produces a uniform beam intensity across the field from the initial forward-peaked beam; an optical distance indicator (ODI), used to find the source-to-surface distance (SSD); a light field, which shows the shape of the expected radiation field; and wedges or trays, used to define the shape of the radiation field. Also, many machines utilize more than one photon treatment energy as well as numerous electron energies. The TomoTherapy HI-ART II unit differs from conventional linacs in that it does not have an ODI, light field, or wedges or trays. It treats using a single photon energy, no electrons, and it also utilizes synchrony of gantry rotation, couch translation, and the opening and closing of the leaves of a binary MLC used to modulate the radiation beam. As previously described, serial tomotherapy can be accomplished with the modification of a conventional linac. However for helical tomotherapy, a completely re-engineered machine was necessary. Therefore, a set of QA guidelines based on those in TG-40 was developed and used to account for variations TomoTherapy has from conventional radiotherapy linacs. The guidelines were designed to test both dosimetric and mechanical aspects of the treatment machine.

These checks can be altered to tailor to a specific treatment center. Some of the tests can be cumbersome to set up and time consuming to collect and store the data. Therefore, TomoTherapy, Inc. has designed a system to collect data in a short, straightforward manner. In this system, a few procedures are performed daily on the treatment machine. Normally, the detector data collected after any procedure run on the machine is stored on the data server and then erased when a new procedure is begun. The new technique, coined TomoTherapy Quality Assurance (TQA), implements software that interfaces directly with the data system after the procedure is run in order to process the detector data. Some of the basic dosimetry modules found on the TQA software include: (1) a step wedge static module in which detector data is gathered from a topographic procedure while an aluminum stepwedge is placed at the end of the treatment couch to attenuate the beam, (2) a rotational variation module in which detector data is collected for a procedure with an unattenuated beam while the gantry constantly rotates allowing users to collect in-air cone profiles, (3) an MLC response module where detector data is gathered from a procedure which utilizes a stationary gantry and a unique MLC sequence, and (4) a data acquisition system (DAS) file system information module collecting machine status information using the same procedure as the rotational variation module. Detector data, specific for each module, is stored on the TQA computer and analyzed over time to help monitor machine performance and possibly predict when a future failure will occur or a part needs to be replaced.

ii. Introduction to the Static Stepwedge

The degradation of the target will result in both energy and off-axis profile changes. As discussed above, variations in off-axis profiles can be monitored by periodic

measurements of in-air or in-water profiles. A third method to monitor the x-ray target is by measuring the attenuation of the beam through an aluminum stepwedge using the exit detector array in association with the TQA software.

The entire TQA system includes the software component as well as a hardware component. The hardware used is an aluminum twinning arm, or stepwedge, that has been developed and used by TomoTherapy in order to make collecting data on the treatment machine more efficient than other methods, such as setting up a water tank. Until recently, the stepwedge has only been used in the factory during the commissioning process of new machines. It was designed to attenuate the beam, followed by collecting of the transmitted signal by the on-board imaging detectors. In this way, properties of the beam could be assessed more efficiently than with an unattenuated beam, and the setup is not as cumbersome as when setting up a water tank. The TQA software processes and stores the detector data. In the clinic, the stepwedge, see Figure 6 and Figure 7, is placed at the end of the treatment couch and progressed through the bore while the gantry remains vertically static at 0°. This is known as a topographic procedure.

a)

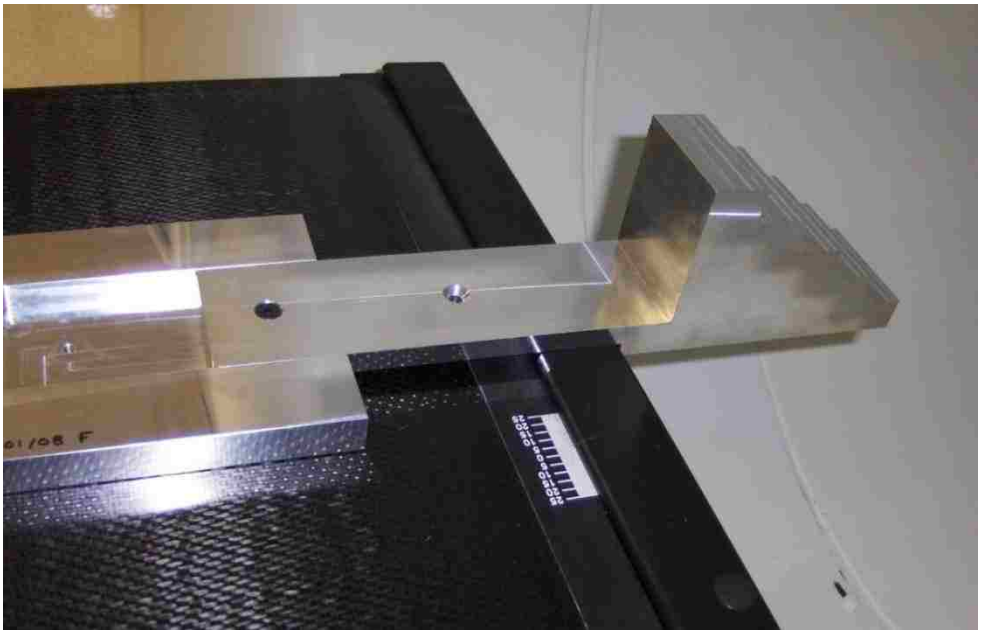

b)

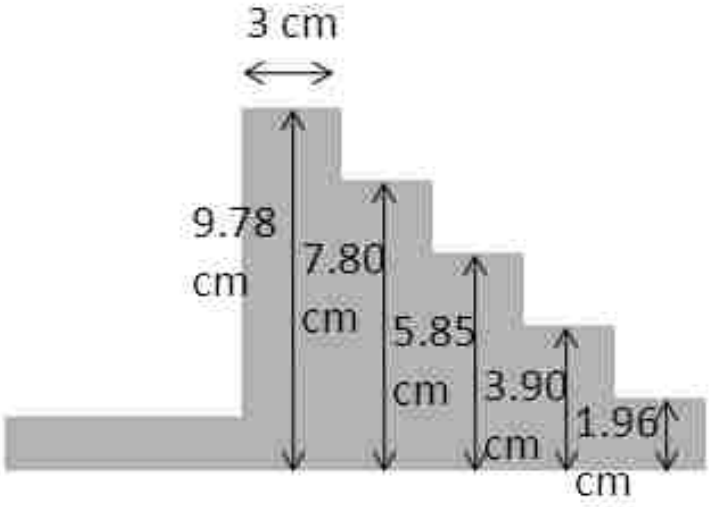

Figure 6**.** a) Photograph of stepwedge overhanging end of treatment couch and b) diagram showing longitudinal width and vertical thickness of each step.

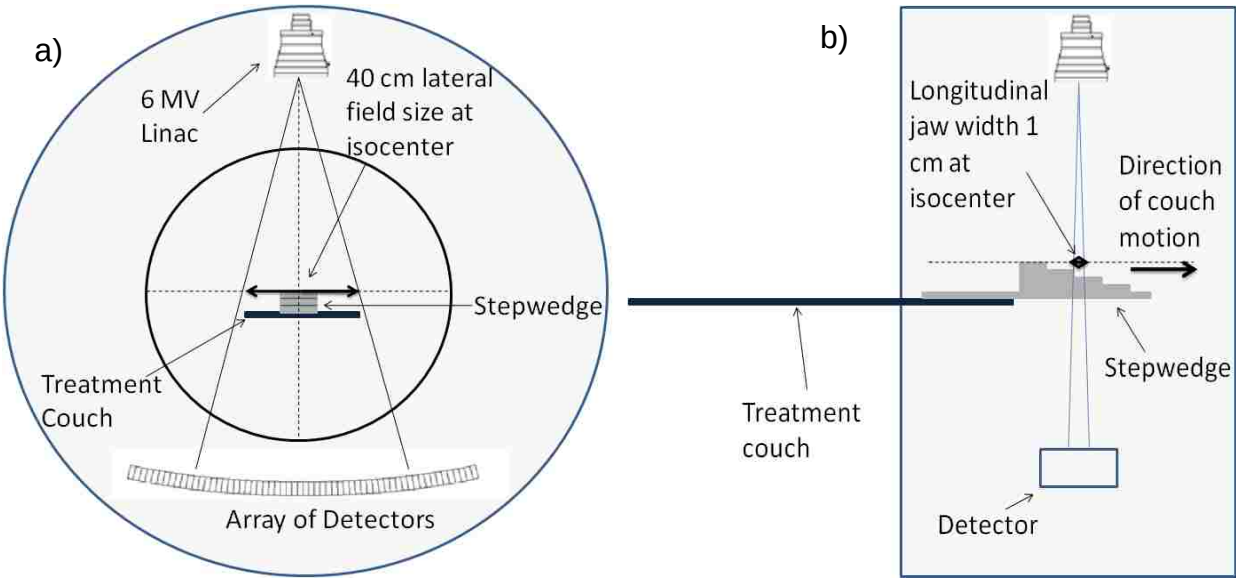

Figure 7**.** a) Axial and b) sagittal view of TomoTherapy unit setup during stepwedge procedure.

II. Hypothesis and Specific Aims

- **Hypothesis**

An effective energy change of 2% can be detected using either attenuation data acquired with an aluminum stepwedge, or water phantom scans of lateral or depth dose profiles.

- **Specific Aims**

Aim 1. Obtain exit detector data daily over lifetime of an x-ray target for a) a rotational variation procedure using an unattenuated beam and b) a topographic procedure using an aluminum stepwedge.

Install rotational variation and static stepwedge procedures onto HI-ART II unit. Obtain and store the exit detector and monitor chamber data from both procedures daily using TQA software provided by TomoTherapy, Inc. over the lifetime of the target. Compute effective attenuation coefficients from the static stepwedge procedure data, and convert these to effective energy using published tables for monochromatic photon beams.

Demonstrate trending describing specific parameters (energy difference) gathered from rotational variation and static stepwedge procedures.

Aim 2. Collect and compare lateral and percent depth-dose (PDD) profiles in water tank monthly.

Obtain lateral and depth-dose profile data for a static HI-ART II beam monthly using Tomo water tank scanning system. Collect lateral profiles for all commissioned jaw widths (1, 2.5, and 5 cm), and at depths 1.5, 5, 10, 15, and 20 cm. Normalize profiles to reference data taken early in target's lifetime and compare with profiles taken throughout target's lifetime.

Aim 3. Collect and compare composite dose data collected from Daily QA plans run each day during daily machine warmup over lifetime of target.

Collect recorded measured dose for a composite IMRT treatment plan, using an A1SL thimble ion chamber inserted in the TomoTherapy cylindrical phantom (TomoPhantom), over the lifetime of the x-ray target. Compare the variation in measured dose over the lifetime of target.

Chapter 2. Methods and Materials

I. Aim 1-Exit Detector Data Collection

A beta version of the TQA software was installed on a laptop provided from TomoTherapy to perform this study. The associated procedure files of each module were loaded onto the TomoTherapy Operator Station and into the database. Modules of the stepwedge static module as well as rotational variation, MLC response, and data acquisition system (DAS) file system info modules were collected daily using the TQA software. The stepwedge static, rotational variation, and MLC response modules were obtained using unique procedures. The DAS file system info module was processed using the data taken from a rotational variation procedure. It collects resulting machine status information from treatment such as temperature, water flow, air pressure, etc.

Table 1. Key parameters for stepwedge static and rotational variation procedures (TomoTherapy 2008).

	Stepwedge	Rot. Var.
Jaw Setting (cm)	1	5
MLC	Open	Open
Couch Speed (mm/sec)	1	Stationary
# of Gantry Rotations	0	10
Beam on Time (sec)	200	200
Data Compression Factor	20	10

The jaw setting for the stepwedge procedure was set to 1 cm to have a reasonably high resolution in the longitudinal direction, whereas the jaw setting was set to 5 cm for the rotational variation to minimize variations with small jaw movements during the procedure. The MLC setting indicates that both of the procedures utilize an open MLC, as opposed to a patient treatment or MLC response procedure in which the MLC modulates the beam throughout delivery. Couch speed is rate of movement in the longitudinal or y direction during the procedure. The number of gantry rotations is the

number of times the gantry rotates through 360°. Beam on time designates the length of the procedure. The detector data compression factor indicates that the raw detector data, taken at 300 pulses/sec using 640 detectors for 200 seconds, is compressed by a factor of 10 or 20. This is done in order to reduce the size of the data file.

For each procedure, the laptop was connected to the Ethernet port of the HI-ART II on-board computer. At the conclusion of each procedure run, the raw data was downloaded from the HI-ART II system to the TQA laptop using file transfer protocol (ftp). The TQA software stores the data and analyzes the results over time.

A. Rotational Variation

The rotational variation QA procedure utilized a rotating gantry and stationary couch with an unattenuated beam. The detector data from a rotational variation procedure is shown in Figure 8a. The detector channel number is shown horizontally. As mentioned previously, there are 640 detector channels. The pulse number is displayed vertically and varies from 0 to 6000 because there are 300 pulses per second, the procedure lasts 200 seconds, and a compression factor of 10 is used. The colors indicate the strength of the exit detector signal with the blue region displaying the lowest signal, green a greater signal, and red the greatest signal.

Figure 8b shows a cross-section through the exit detector data for a single pulse. The shape of the cone profile for a single pulse, or averaged over several rotations, is used to determine beam constancy. After the rotational variation procedure is run, both a rotational variation and DAS file system info module are processed using the TQA software.

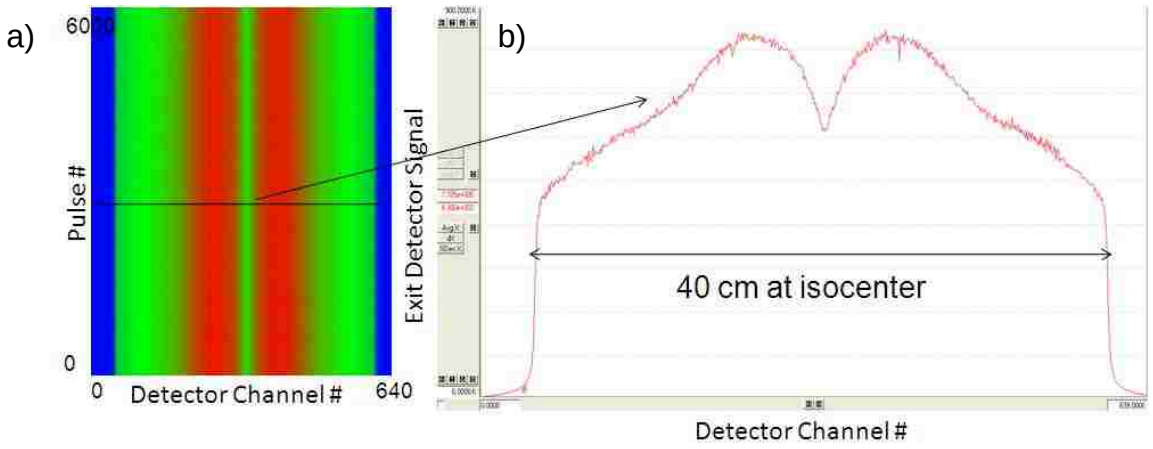

Figure 8**.** Exit detector data from a rotational variation procedure. (a) Two-dimensional array of exit detector data versus channel and pulse number and (b) cone profile from one lateral pulse of the exit detector.

B. Static Stepwedge

The static stepwedge procedure is run with the aluminum stepwedge placed at the end of the treatment couch, centered laterally and its top surface placed at the height of a horizontal line through isocenter. The stepwedge is placed so that the long axis is orientated longitudinally and the edge of the first step is 50 mm in front of the beam plane, see Figure 6 and Figure 7. The aluminum stepwedge has steps that are 7 cm wide in the lateral or x dimension and 3 cm long in the longitudinal or y dimension.

The beam attenuation depends on the thickness of each step in the stepwedge. Measurements were made of the thickness using calipers. The determined thicknesses in the vertical or z dimension are displayed in Table 2, where the variances displayed are the standard deviation of the sample.

The stepwedge procedure also utilizes a couch setup-to-movement offset of 1 cm which indicates the initial couch movement after setup is complete. It is done because the couch error tolerance is proportional to the initial distance of movement.

Table 2. Thickness of individual steps of the aluminum stepwedge.

Step #	Thickness (cm)
1	1.96 ± 0.0099
2	3.90 ± 0.0039
3	5.85 ± 0.0049
4	7.80 ± 0.0024
5	9.78 ± 0.022

For example, the error tolerance on setup parameters was set to ±1%. Therefore, if the couch were supposed to initially move 1 cm, the error tolerance would be 1 cm ± 0.01 cm. This results in a tighter tolerance for longitudinal errors over typical patient treatment procedures, which have couch setup-to-movement offsets of about 50 cm.

Once the procedure is complete, the TQA software downloads the system data for analysis. For the stepwedge module, several system checks are made in addition to our main focus, monitoring the constancy of the attenuation coefficients. Some of the variables processed for the stepwedge module include:

Edge Slope Average-a linear fit is performed for the signal along the central channels at each step edge. The average slope of these linear fits is reported and represents a measure of the consistency of the couch speed.

IECx Offset-A 1D array of step-wedge centers is calculated by iterating across the stepwedge detector data and determining the FWHM center for each pulse. The median of this array is then compared to that of the reference to determine a relative offset.

IECy Offset-A 1D array of edge locations is calculated by searching for the location of the mid attenuation level between each consecutive step. The array is then normalized by the speed ratio and subtracted from the reference edge

location array. The average difference is then reported.

IECz Offset-A 1D array of stepwedge widths is calculated by iterating across the stepwedge detector data and determining the FWHM width for each pulse. The median of this array is then compared to that of the reference to determine a relative offset.

Speed Difference-Edge locations are calculated by searching for the location of the mid-attenuation level between each consecutive step. The distance between consecutive edge locations define a step length. Lengths determined for each step are then compared to the reference set and the average difference is reported.

Energy Difference-the main component of the TQA system to be monitored for the stepwedge module. The linear attenuation coefficient, which can be used to determine energy, is calculated using the detector data gathered from the stepwedge procedure. The software does not display the effective energy or even the measured effective linear attenuation coefficient. It calculates the attenuation coefficient and then displays a percent change from a reference over time. First, the user is required to define a reference. Over time, the measured linear attenuation coefficient determined from the exit detector data for each procedure is compared to this reference.
Exit detector data from example stepwedge procedures are shown in Figure 9. The figure shows lateral profiles of the detector data, taken for one pulse and using all 640 detectors. Figure 9a shows the profile through the unattenuated portion of the procedure, i.e. data prior to the stepwedge moving into the path of the beam. Figure 9b illustrates a cone profile obtained when the beam is centered on one of the individual steps. Both profiles are similar to an unattenuated cone profile in their shape and central dip, however the difference between the two is that Figure 9b has a well

surrounding the central dip, due to the stepwedge. Each step thickness is different and therefore the well would be deeper or shallower depending on which step the lateral profile was taken through.

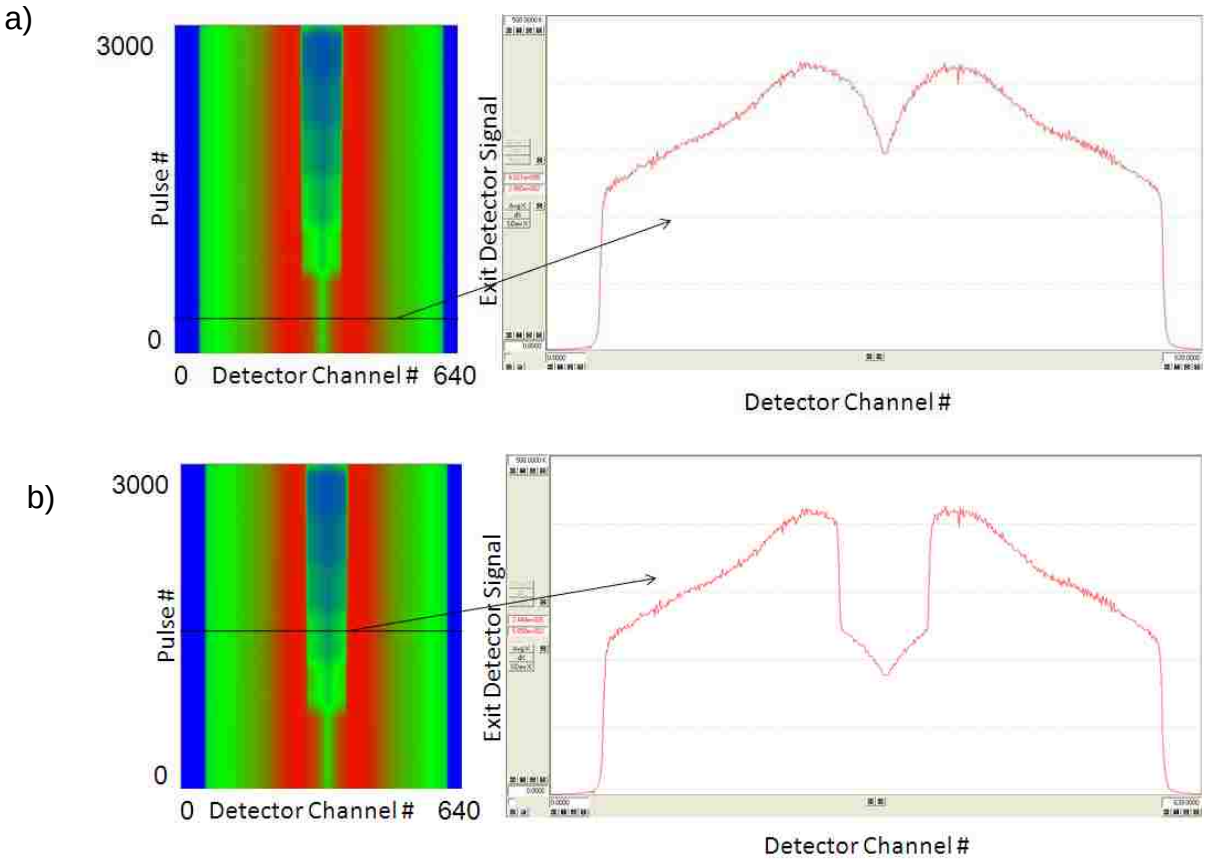

Figure 9**.** Exit detector data from stepwedge procedure. Lateral profile taken for a single pulse for a) a pulse prior to the stepwedge moving into the path of the beam and b) a slice obtained when the beam is centered on one of the individual steps.

Using the lateral profile, the TQA software determines the location of each edge of the wall that the stepwedge produces. The location halfway between these two edges is used as the center of attenuation. Then, a longitudinal profile of the exit

detector data is plotted through the location of the center of attenuation. This is shown in Figure 10.

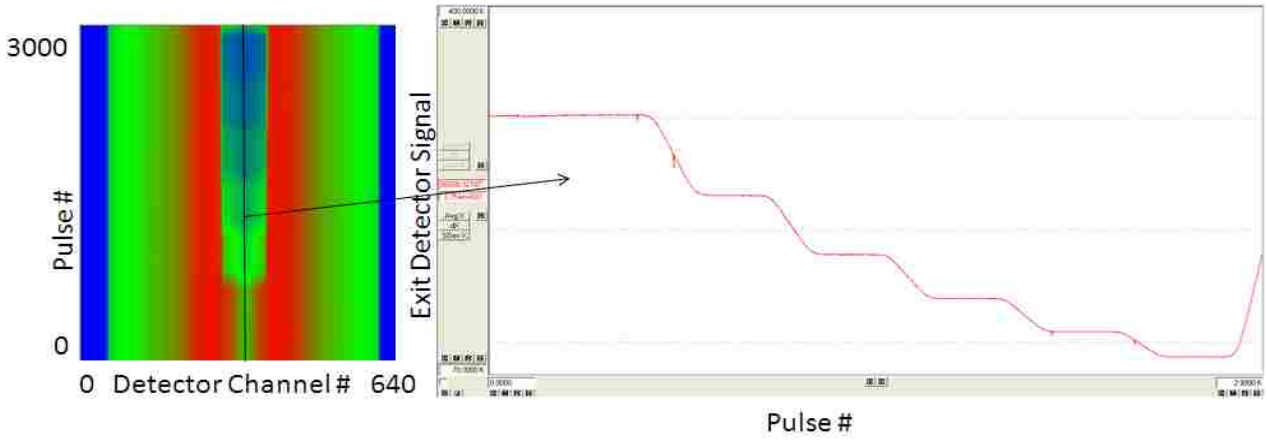

Figure 10. (a) Exit detector data from the stepwedge procedure and (b) longitudinal profile through center of attenuation.

The largest exit detector signal, due to the unattenuated beam, is shown at the earlier pulse values. As the pulse number increases, the beam passes through thicker steps of the wedge, (see Figure 6) seen by the five subsequent steps. This attenuation data is used to determine the linear attenuation coefficient from the equation:

$$I = I_o e^{-\left(\frac{\mu}{\rho}\right)(\rho x)}, \qquad (1)$$

where:

I = Intensity of the beam

I_o = Unattenuated intensity of the beam

μ = Linear attenuation coefficient for aluminum (cm^{-1})

ρ = Density of aluminum (2.7 g/cm^3)

x = Thickness of a given step of the wedge (cm)

From the data gathered in Figure 10, I_o and I can be determined. Each are the average of the central 100 pulses for a given step. Rearranging equation 1 gives:

$$-\ln\left(\frac{I}{I_o}\right) = \mu x, \tag{2}$$

Plotting $-\ln\left(\frac{I}{I_o}\right)$ vs. the thickness of each step and using a linear fit to determine the slope, yields μ. This is illustrated in Figure 11. In the TQA software, linear fit is constrained to go through the origin.

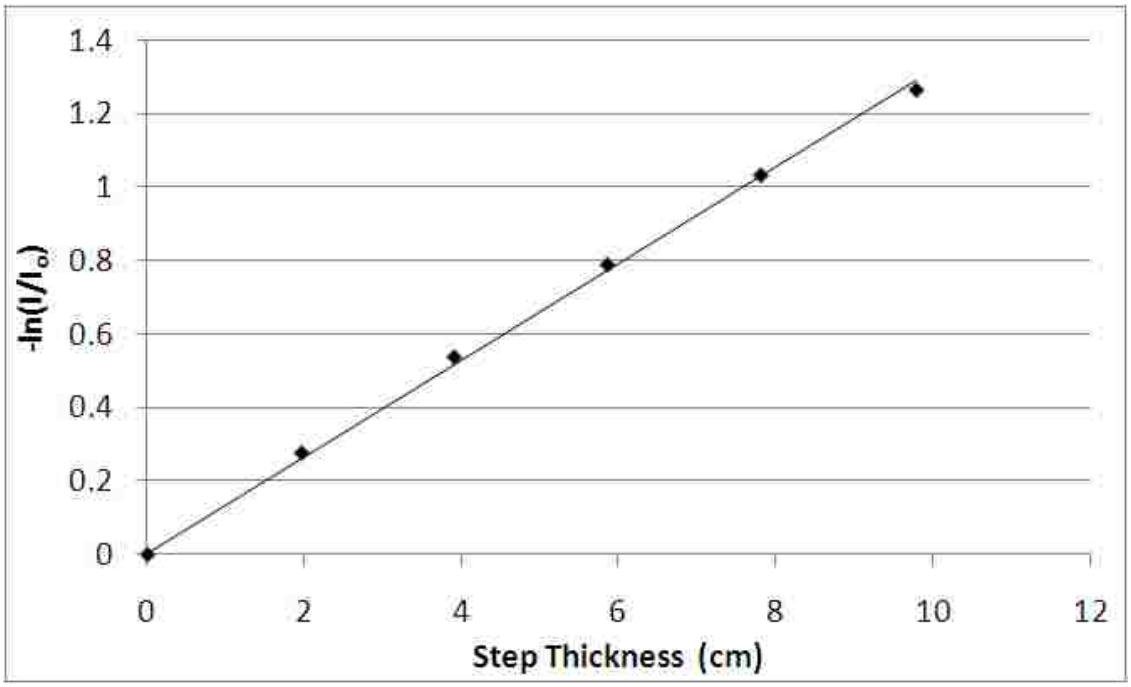

Figure 11**.** Fit of thickness of steps vs. attenuation through steps, $-\ln\left(\frac{I}{I_o}\right)$ plotted vs. stepwedge thickness and fit linearly to determine μ.

The attenuation coefficient is a function of the effective energy of the beam. In this work, we have used the Hubbell and Seltzer (Hubbell and Seltzer 2004) theoretical model for relating the two, see Figure 12.

Photon Energy (MeV)	μ (cm^{-1})
0.1	0.46008
0.15	0.37206
0.2	0.33021
0.3	0.28134
0.4	0.250452
0.5	0.228015
0.6	0.210654
0.8	0.184707
1	0.165942
1.25	0.148392
1.5	0.135162
2	0.116748
3	0.095607
4	0.083862
5	0.076572
6	0.071685
8	0.065799
10	0.062586
15	0.059265
20	0.058536

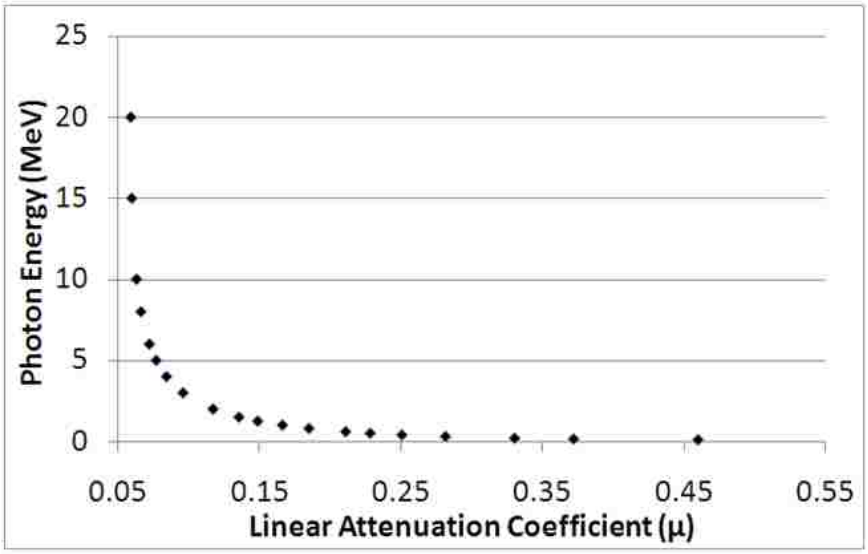

Figure 12. Photon energy and corresponding linear attenuation coefficient for aluminum.

The linear attenuation coefficient was converted to effective energy for each measured reading. Each measured linear attenuation coefficient and corresponding energy had an error associated with it. To determine the uncertainty of the measurements, a least squares fit to a second-order polynomial (Bevington and Robinson 1992) was applied to a portion of the data collected from July 19, 2008 to November 4, 2008. This range was chosen because it fell in the linear portion of the data. To test how accurate a second order least squares fit was to the set of data, a goodness of fit test was assessed using the correlation coefficient, r^2 defined as:

$$r^2 = 1 - \frac{SSE}{SST}, \tag{3}$$

where:

SSE = Sum of squares of distances from measured data to fit data.

SST = Sum of distance from measured data to mean of measured data squared.

A perfect correlation would yield an r^2 of 1 indicating that the fit exactly represents the variable where a fit which has no correlation would yield an r^2 of 0. In our case, r^2 was calculated to be .9752. This indicated that 97% of the variation in the measured data could be explained by the fit, while the other 3% was of unknown origin. In general, an r^2 greater than 0.75 shows a strong correlation, an r^2 between 0.5-0.75 indicates a moderate correlation, and an r^2 less than 0.5 shows a weak correlation. Therefore, the second order polynomial fit model was determined to be accurate to determine the variance.

To determine the error, a reduced chi squared technique was applied using a second order least squares fit model (Bevington and Robinson 1992).

$$\frac{\chi^2}{\nu} = \frac{1}{N-1}\sum_{i=1}^{N}\frac{[y_i - f(x_i)]^2}{\sigma^2}, \quad (4)$$

where:

N = Number of data points

y_i = Measured data point

$f(x_i)$ = Calculated data point using least squares fit model

σ^2 = Variance in measured data point

ν = Number of degrees of freedom

Three assumptions were made: $\frac{\chi^2}{\nu}$ was equal to 1, σ was the same for all data points, and the linear attenuation coefficient or effective energy was directly related to time. The error, σ, was determined by setting $\frac{\chi^2}{\nu}$ equal to one and solving for σ directly.

Using the data shown in Figure 12 and the error in the measured reading, the sensitivity to energy change could be defined quantitatively. Figure 12 shows energy versus linear attenuation coefficient for energies ranging from 0.1-20 MeV. However, the change over the lifetime of the target was much narrower. Once this range was determined from the measurements, only those values bounding the data taken would be included. A linear fit was applied to these values and the slope determined. The slope assumed that the linear attenuation coefficient was plotted on the y-axis and the effective energy on the x-axis. This is contrary to what Figure 12 shows. Using this slope and the measured error in linear attenuation coefficient just described, a sensitivity to energy could be determined as follows:

$$S = \frac{\sigma_\mu}{m}, \tag{5}$$

where:

S = Sensitivity to energy change (MeV)

m = Slope of linear attenuation coefficient vs. photon energy ($cm^{-1}*MeV^{-1}$)

σ_μ = Error in linear attenuation coefficient (cm^{-1})

The error in the slope was determined from the equation (Bevington and Robinson 1992):

$$\sigma_m^2 = \frac{1}{\Delta}\sum_{i=0}^{N}\frac{1}{\sigma_\mu^2}, \tag{6}$$

where:

σ_m = Error in slope (MeV)

$$\Delta = \sum \frac{1}{\sigma_\mu^2} \sum \frac{x_i^2}{\sigma_\mu^2} - \left(\sum \frac{x_i}{\sigma_\mu^2}\right)^2$$

σ_μ = Error in linear attenuation coefficient (cm^{-1})

x_i = Value of linear attenuation coefficient (cm^{-1})

Additionally, to test the sensitivity of the stepwedge procedure to known changes in energy while also eliminating target degradation factors, the procedure was run several times while manually varying the injector current. This was done on April 11, 2009, after a new target had been installed. The stepwedge was setup the same way as when taking a measurement on any day throughout the lifetime of the target. The injector current setting was varied up to the maximum and minimum that the system would allow without interlocking and the procedure was performed at these settings as well as a few in between.

MLC response, the third module, procedures were collected over the lifetime of the target but were not used for the study.

II. Aim 2-Lateral and Percent Depth Dose Profile Collection

Lateral and percent depth dose (PDD) profiles were collected monthly using a water tank system. This system operates using two ion chambers, the Tomo water tank and scanner, picture and schematic shown below in Figure 13; and the TomoTherapy Electrometer Measurement System (TEMS)(Standard Imaging, Madison, WI) software. The multichannel electrometer used houses 8 channels and is capable of measuring collected charge every 100 milliseconds.

The water phantom was set up for an 85 cm SSD measurement. The tank was set up on the treatment couch so that the longer side was in the x direction. After the scanning arm attachment was connected to the tank, it was secured and leveled in the lateral and longitudinal direction using three large black screws, two on the top left side and one on the bottom right. A ruler was placed under the +y side of the tank in order to correct for slight couch sag when inside the bore. The tank was aligned to the green, isocentric lasers.

To level the tank, bubble levels were placed on top of the sides of the tank and on the scanning arm attachment. The scanning ion chamber (Model A1SL Exradin Miniature Shonka Thimble Chamber) was inserted into the chamber mount attached to the scanning arm. It was positioned so that the end of the chamber was 4 mm past the axial laser. For reference, a CT ion chamber (Model A17 Exradin CT Chamber) was mounted on the front step on the side of the tank, outside the field. Once mounted, the chamber was raised and lowered to ensure that it did not drift vertically and adjusted horizontally to make sure it did not move in or out of the water. This was also done with the tank inside of the bore in order to account for possible couch sag. Once the tank was properly leveled, an MVCT with the ion chamber at water surface level was done to check proper alignment.

All profiles were taken with the MLC leaves open and a fixed gantry setting of 0°. Each lateral profile, the ion chamber scanning horizontally over the transverse width of the beam, was taken for 1, 2.5, and 5 cm jaw settings and at depths of 1.5, 5, 10, 15, and 20 cm. PDD profiles were taken along the central axis for the three jaw settings. PDD was defined as the quotient, expressed as a percentage, of the absorbed dose at

any depth d to the absorbed dose at a fixed reference depth d_o, along the central axis of the beam (Khan 2003).

$$PDD = \frac{D_d}{D_{d_o}} x\ 100, \qquad (7)$$

The reference depth was taken as the depth of maximum dose for a given beam. Readings were taken using a scanning ion chamber and a reference CT ion chamber. The scanning chamber has a collecting volume of 0.057 cm^3 and the reference chamber a collecting volume of 1.91 cm^3. The raw data from the scanning A1SL ion chamber was normalized to the reference CT ion chamber to account for possible fluctuations in machine output. The scanning chamber was driven in the tank to the specified depths using the water tank scanner and TEMS system. Profiles were displayed using the software but could also be exported to an external data analysis software in order to plot cumulative data onto one chart for comparison.

A. Lateral Profiles

Lateral profile readings were normalized to the value on the central axis then plotted vs. horizontal position. Example lateral profile data for the 2.5 cm jaw and depth of 1.5 cm are shown in Figure 14. Lateral position is displayed horizontally and the normalized reading vertically.

The triangular shape of the profile is due to the absence of a flattening filter on the TomoTherapy unit. In the 6 MV linear accelerator a narrow beam of electrons passes through an exit window, after which it strikes a high-z target producing a forward-peaked x-ray beam due to the forward ratio of bremsstrahlung cross section.

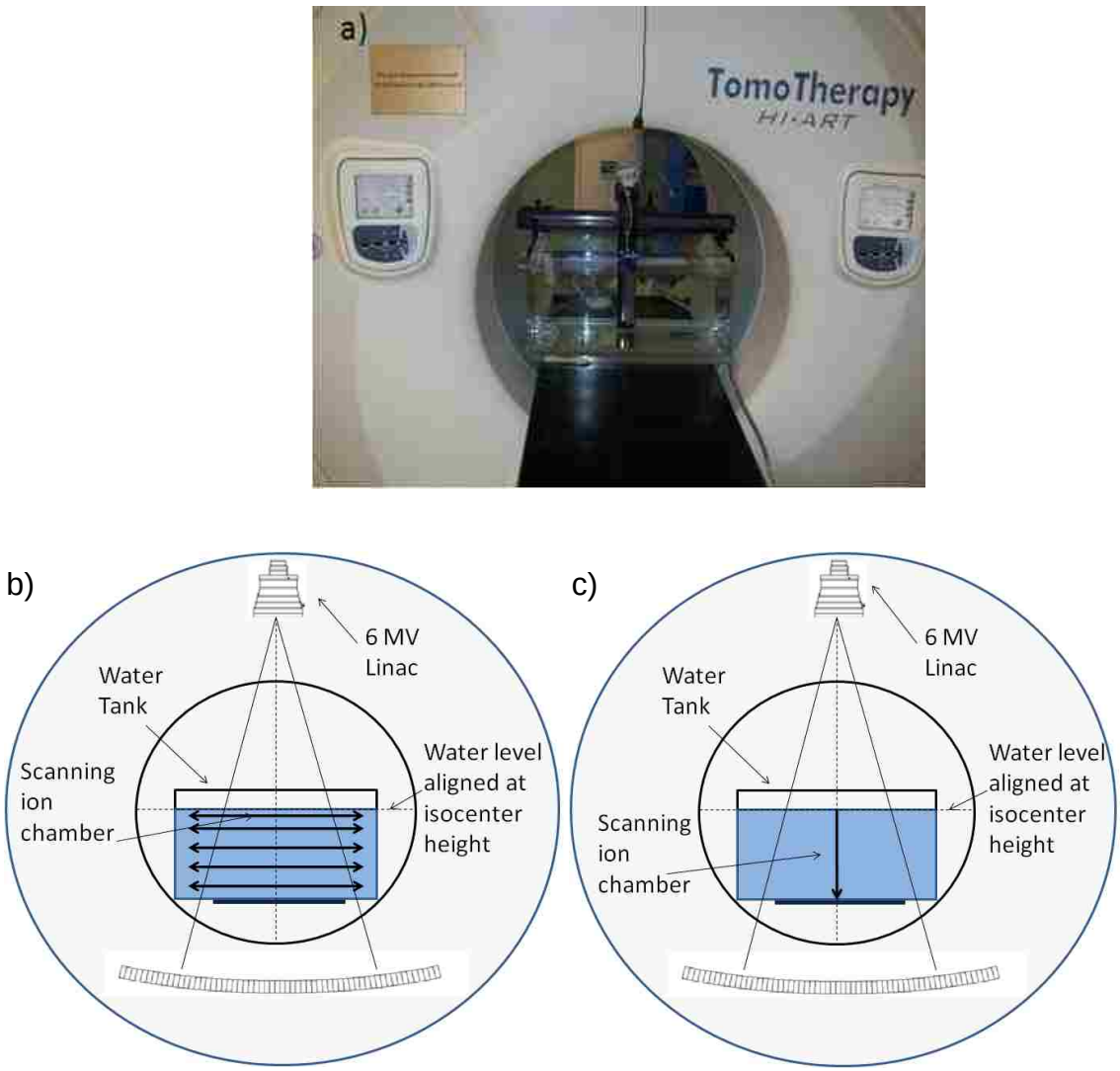

Figure 13**.** Water tank setup. a) Photograph of water tank scanning system inside the bore of the machine, b) axial diagram of the setup used to collect lateral profiles, and c) axial diagram of setup used to collect percent depth dose (PDD) profiles.

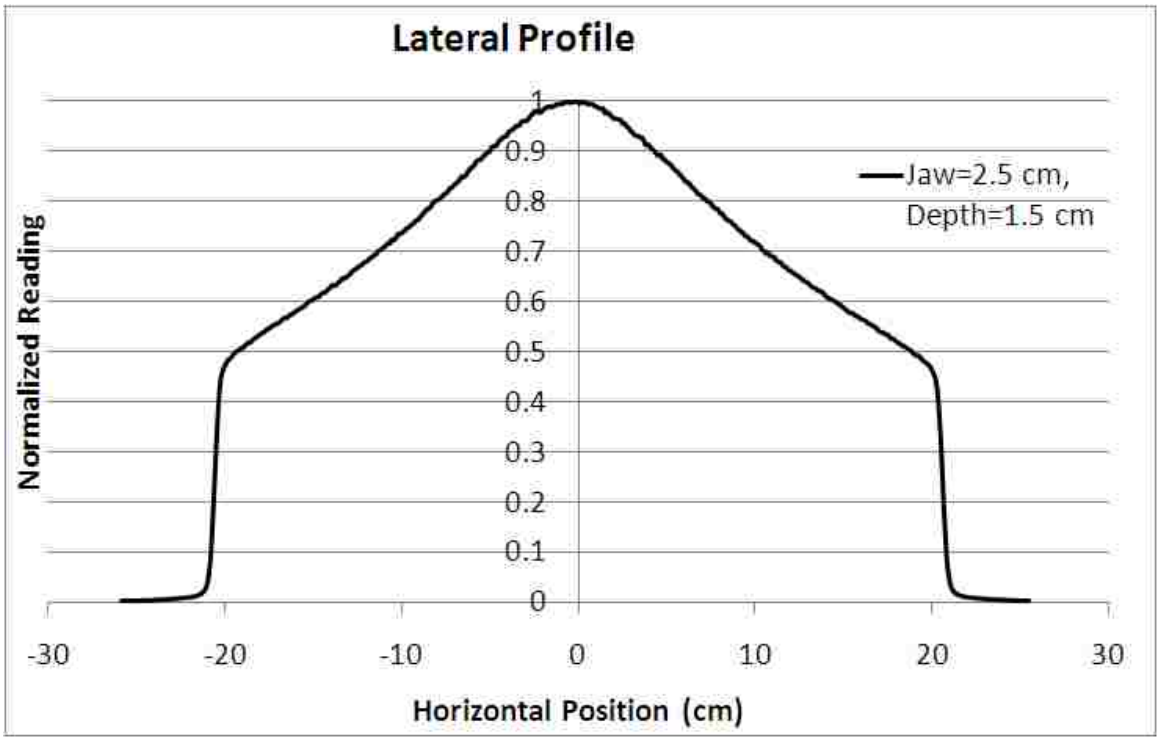

Figure 14. Lateral profile taken using the TEMS system and water tank. Data gathered at 85 cm SSD, depth=1.5 cm, jaw setting=2.5 cm.

On conventional machines, in order to make the beam uniform in lateral intensity, the beam passes through a low-z flattening filter. This filter acts to absorb relatively more of the high intensity radiation found closer to the central axis to make the intensity of the field more uniform (or flat) across the field (Greene 1986). This was necessary on a conventional linac for treatments designed for broad, unmodulated beams. However, a flattening filter is not necessary on a machine designed specifically for IMRT. On TomoTherapy, the flattening filter is absent and is not needed since the gantry rotates and the beam is constantly modulated by the MLC throughout treatment. If during treatment planning, the optimizer were to select a uniform energy fluence distribution to deliver, the MLC is capable of modulating the distribution to be uniform. Advantages of a lack of a field-flattening filter include less head scatter, less differential

hardening of the beam across the field, and higher dose output resulting in shorter treatment time (Mackie and Olivera 2003); (Fenwick, Tome et al. 2004).

The profile collected using the water tank system in which the beam scans across the transverse plane is a lateral or cone profile. The lateral profiles collected for the scans taken over the lifetime of the x-ray target are shown in Figure 15.

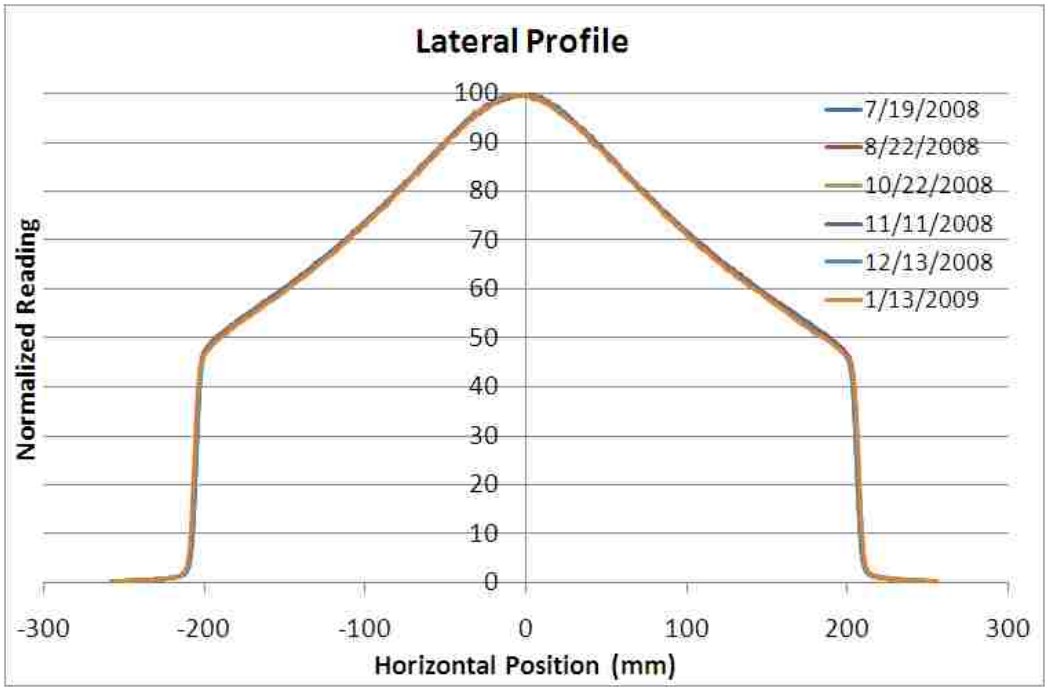

Figure 15. Lateral profiles taken using the TEMS system and water tank over the lifetime of the x-ray target. Jaw=2.5 cm, Depth =1.5 cm.

To better visualize the small differences between the measured profiles, the percent differences of each profile from a reference profile were calculated at all horizontal positions within ±200 mm. This was done using a reference scan chosen early in the target lifetime, July 19, 2008 in our case. Shown in Figure 16 are the percent differences from reference for each scan.

Percent difference, Δ%, was calculated using the equation:

$$\Delta\%(x) = \frac{[Rdg(x) - Rdg_{ref}(x)]}{Rdg_{ref}(x)}\ x\ 100\%, \quad (8)$$

where:

$Rdg(x)$ = Normalized reading for a lateral point, x, taken for each monthly scan

$Rdg_{ref}(x)$ = Normalized reading for a lateral point, x, taken at reference

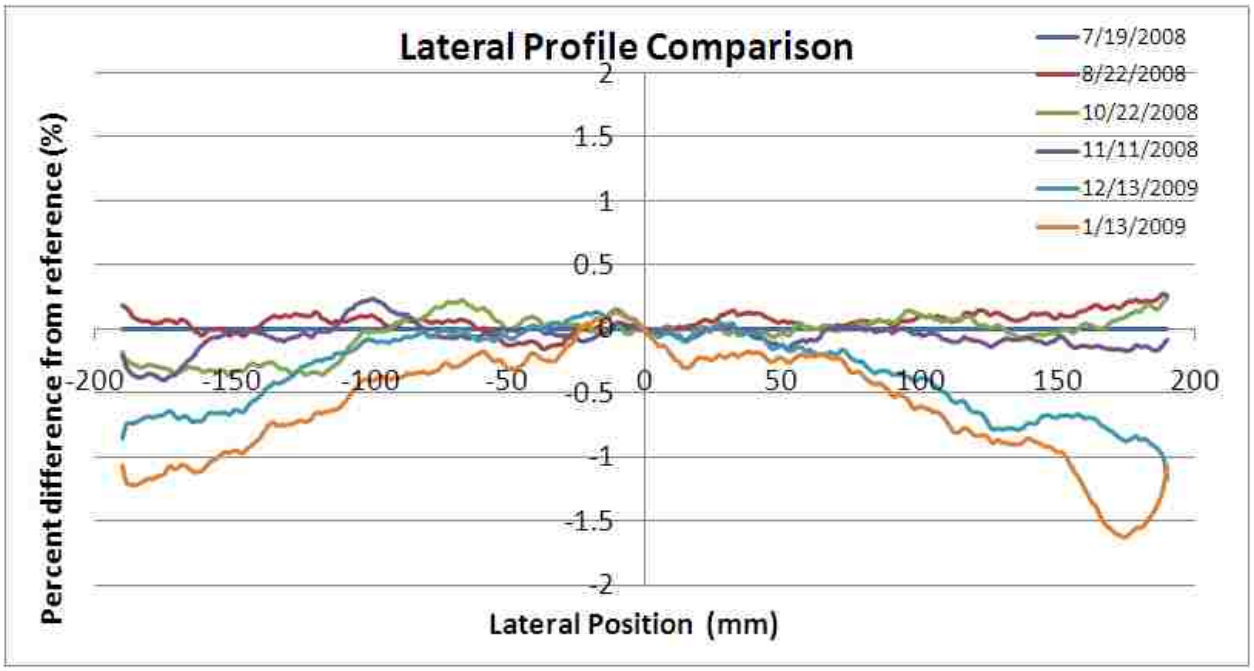

Figure 16. Percent difference from reference (7/19/2008) for lateral profiles.

For each monthly scan measured, the average off-axis ratio (OAR) for ±15 cm was calculated. First, the maximum normalized reading was determined along with its associated horizontal position. Although expected to be at the central axis, this peak was typically slightly off-center. Once the horizontal position of the peak was determined, the ionization readings at ±15 cm from this position were found and used to calculate the average off-axis ratio. This was defined as the average reading at x≈15 and x≈-15 cm divided by the reading at the peak, i.e.:

$$Avg.OAR = \frac{Rdg(15) + Rdg(-15)}{2\ x\ Rdg(0)}, \quad (9)$$

To reduce the effects of noise on the results, a fit was used to smooth the lateral profile curve. For points at 15 cm and -15 cm, the off-axis value was found from a linear fit to the points within 1 cm of 15 and -15 cm, respectively. The horizontal position of the peak value was found from a second order polynomial fit using the points within 1 cm on either side. These are illustrated in Figure 17 for a profile at depth 1.5 cm using a 2.5 cm jaw. In this example, the position of the peak value would be shifted by -0.25 cm. Therefore the ionization readings to be incorporated into the OAR would be 14.75 cm and -15.25 cm.

The next step was to determine the error bars in the OAR. The OAR consisted of three variables: the readings at 15 cm, 0 cm, and -15 cm. Each measured reading had an associated error and the fit through the measured readings had an associated error. The error in the measured readings was found using the chi-squared method described in Aim 1. This error was substituted into equation 5. Also, an error in the fit had to be determined as it was the value used in the OAR calculation. The error in the fit reading was estimated using the following method.

$$\sigma^2 = \frac{\sigma_{data}^2}{\nu}, \quad (10)$$

where:

σ_{data}^2= Estimated error in an individual measured data point.

ν = Number of data points – number of parameters.

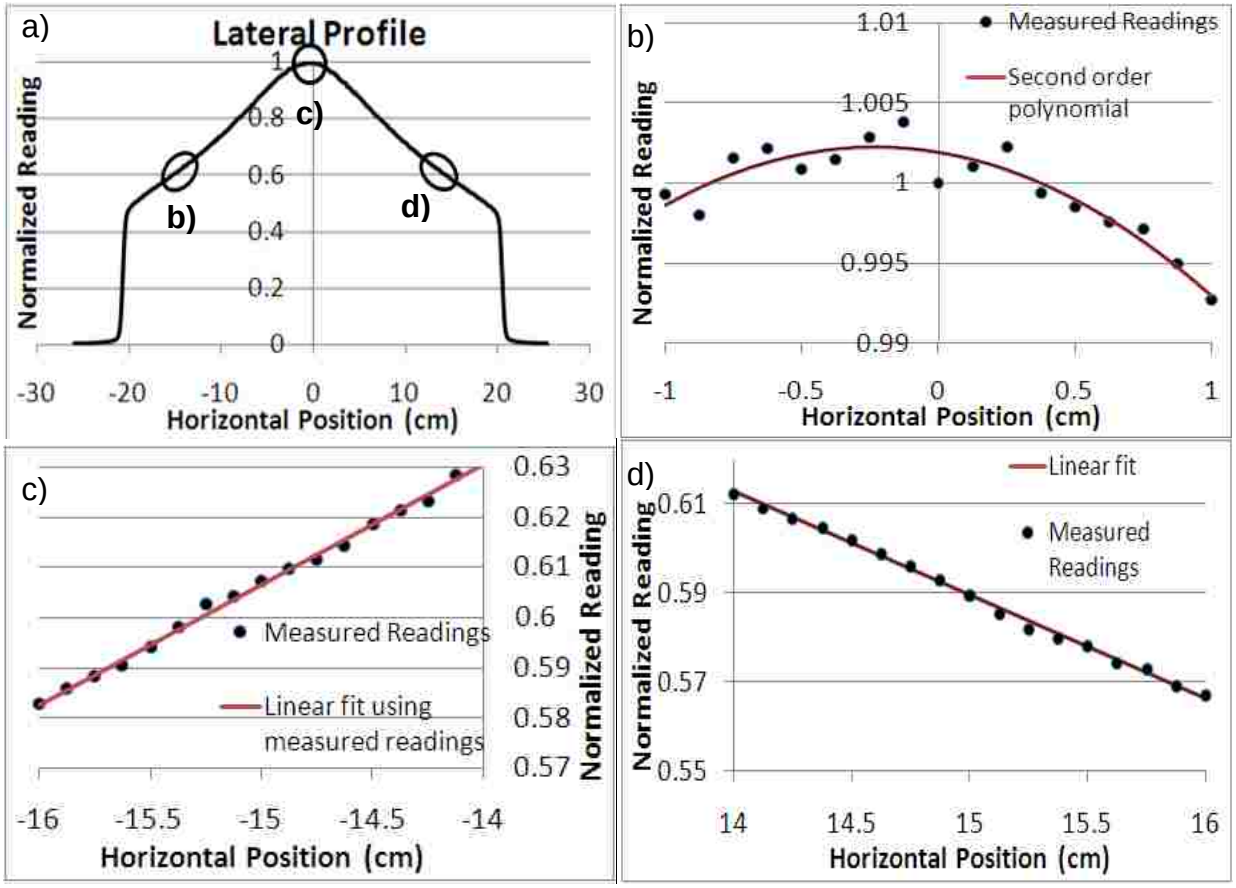

Figure 17**.** Lateral profiles showing where fits are applied to determine off-axis ratio. a) Normalized lateral profile with circled regions indicating where off-axis ratios are determined; b) readings and second order polynomial fit for 1 cm on either side of the central axis c) measured readings and linear fit for 1 cm on either side of -15 cm;; and d) readings and linear fit for 1 cm on either side of 15 cm.

Once the error for each component of the OAR was found (equation 10) the total error in the OAR (equation 9) was propagated. The total error is given by:

$$\sigma_{OAR}^2 = \left(\frac{\partial OAR}{\partial Rdg(15)}\right)^2\sigma_{Rdg(15)}^2 + \left(\frac{\partial OAR}{\partial Rdg(-15)}\right)^2\sigma_{Rdg(-15)}^2 + \left(\frac{\partial OAR}{\partial Rdg(0)}\right)^2\sigma_{Rdg(0)}^2, \qquad (11a)$$

Substituting partial derivatives back into equation 11a:

$$= \frac{OAR^2}{[Rdg(15)+Rdg(-15)]^2}\left(\sigma_{Rdg(15)}^2 + \sigma_{Rdg(-15)}^2\right) + \frac{OAR^2}{Rdg(0)^2}\sigma_{Rdg(0)}^2, \qquad (11b)$$

Dividing each side by OAR^2 and taking the square root:

$$\frac{\sigma_{OAR}}{OAR} = \sqrt{\frac{[\sigma^2_{Rdg(15)} + \sigma^2_{Rdg(-15)}]}{[Rdg(15)+Rdg(-15)]^2} + \frac{\sigma^2_{Rdg(0)}}{Rdg(0)^2}}, \quad (12)$$

As was done for the stepwedge, a way of quantitatively determining the sensitivity of the OAR data as a function of change in energy was required. Therefore, the off-axis ratios were plotted versus the effective energy measured using the stepwedge procedure. A linear fit was applied and the slope determined. When determining the slope, it was assumed that the OAR was plotted on the y-axis and the effective energy on the x-axis. This was contrary to the way that the data was plotted in the results. Using this slope and the measured error, the sensitivity of OAR to energy change was estimated:

$$S = \frac{\sigma_{OAR}}{m}, \quad (13)$$

where:

S = Sensitivity to energy change (MeV)

m = Slope of effective energy vs. OAR (MeV^{-1})

σ_{OAR} = Error in OAR

The error in the slope was determined in the same way as equation 6 with the OAR replacing the linear attenuation coefficient.

B. Percent Depth Dose (PDD) Profiles

A way to quantitatively compare PDD scans taken on various dates was again required. The method used was based on the technique for assessing beam quality in standard dose calibration protocols, e.g. the method in TG-51 (Almond, Biggs et al. 1999). Specifically, the ratio of the ionization reading at 15 cm to 5 cm depth would be used to compare each scan, similar to the OAR averages used for comparing lateral profiles. The exact values at each depth were not used, as there could be noise

associated with a given reading at depth. Therefore, a fit was applied to the data to determine the two depths used, 5 cm and 15 cm. The fit used was designed to account for exponential as well as inverse square effects. It was modeled using the relation:

$$PDD\ \alpha\ \frac{e^{-(\mu\,(d-d_{max}))}}{(85+d)^2}, \tag{14}$$

where μ is the linear attenuation coefficient (cm^{-1}), d the depth in water (cm), d_{max} the depth of maximum dose (cm), and 85 the SSD of the water tank setup in cm.

The fits included data within 2 cm on either side of the desired depths, 5 and 15 cm, on the PDD curve, i.e. 3-7 cm and 13-17 cm respectively. These regions are illustrated in Figure 18.

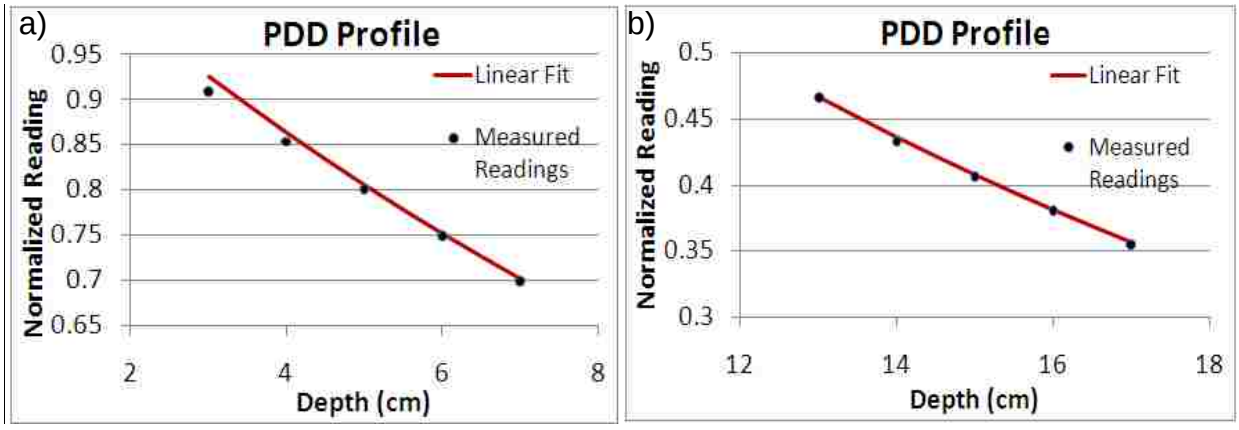

Figure 18. Regions of PDD profile where fits of 5 cm and 15 cm were applied. a) Measured readings and PDD fit for 5 cm depth and b) readings and PDD fit for 15 cm depth. Jaw Width=2.5 cm

The error bars in the ratio were determined similar to that done for the OAR, e.g. for $Ratio_{15/5}$:

$$\sigma^2_{Ratio_{15/5}} = \left(\frac{\partial Ratio_{15/5}}{\partial Rdg(5)}\right)^2\sigma^2_{Rdg(5)} + \left(\frac{\partial Ratio_{15/5}}{\partial Rdg(15)}\right)^2\sigma^2_{Rdg(15)}, \tag{15}$$

Rearranging terms:

$$\frac{\sigma_{Ratio_{15/5}}}{Ratio_{15/5}} = \sqrt{\frac{\sigma Rdg(5)^2}{Rdg(5)^2} + \frac{\sigma Rdg(15)^2}{Rdg(15)^2}}, \quad (16)$$

Where $Ratio_{15/5}$ is the ratio of the ionization reading at 15 cm depth to the ionization reading at 5 cm depth, $Rdg(5)$ is the ionization reading at 5 cm depth, and $Rdg(15)$ is the ionization reading at 15 cm depth.

Again, a way of quantitatively comparing PDD to energy was required. As was done for the OAR, the PDD ratios were plotted versus effective energy. The data was fit linearly and the slope determined. The slope assumed that the PDD ratios were plotted along the y-axis and the energy on the x-axis. This slope, along with the error measured in the ratio, was used to find the sensitivity to energy change in MeV:

$$S = \frac{\sigma_{Ratio_{15/5}}}{m}, \quad (17)$$

where:

S = Sensitivity to energy change (MeV)

m= Slope of effective energy vs. $Ratio_{15/5}$ (MeV^{-1})

$\sigma_{Ratio_{15/5}}$ = Error in $Ratio_{15/5}$

The error in the slope was measured in the same way as done for equation 5 with the $Ratio_{15/5}$ replacing the linear attenuation coefficient.

As was done for the first aim, manual injector current adjustments were made during a single setup in order to test sensitivity to known energy change. Both lateral and PDD profiles were collected for multiple injector current settings.

II. Aim 3-Composite Plan

To provide an independent assessment of whether a change in energy as determined from the prior two aims affected a simulated patient treatment delivery, an IMRT QA plan was delivered and measured daily. Each day prior to patient treatment, Daily QA procedures are run in order to warm-up the machine as well as test to ensure it is performing within defined tolerance. One of the daily procedures used to simulate a patient treatment is an IMRT treatment plan (Figure 19a) delivered to the Tomo cheese phantom (Figure 19b). This composite check plan utilizes a rotating gantry, moving couch, and modulated MLC leaf sequence file to simulate the helical delivery used during IMRT treatment delivery. The longitudinal collimating jaws are set to 2.5 cm. An ion chamber was inserted at a specific position in the phantom in order to measure the delivered dose. Each day that the plan was run, the measured dose delivered to a phantom was recorded. It was compared to the stepwedge and lateral and PDD profile data.

The calculated delivered dose for the composite plan was 1.97 Gy. This was compared to measured dose collected using the TomoPhantom and one A1SL ion chamber (Model A1SL Exradin Miniature Shonka Thimble Chamber). The chamber has a collecting volume of 0.057 cm^3 and was located at +10.5 cm on the x-axis. The ion chamber readings were taken on an electrometer (Keithley Model 614) connected to the chamber through triaxial cable.

The measured dose was calculated following the formalism of the TG-51 protocol (Almond, Biggs et al. 1999):

$$D_M = M_{raw} P_{ion} P_{TP} P_{elec} P_{pol} k_Q N_{D,w}^{60_{Co}}, \quad (18)$$

a)

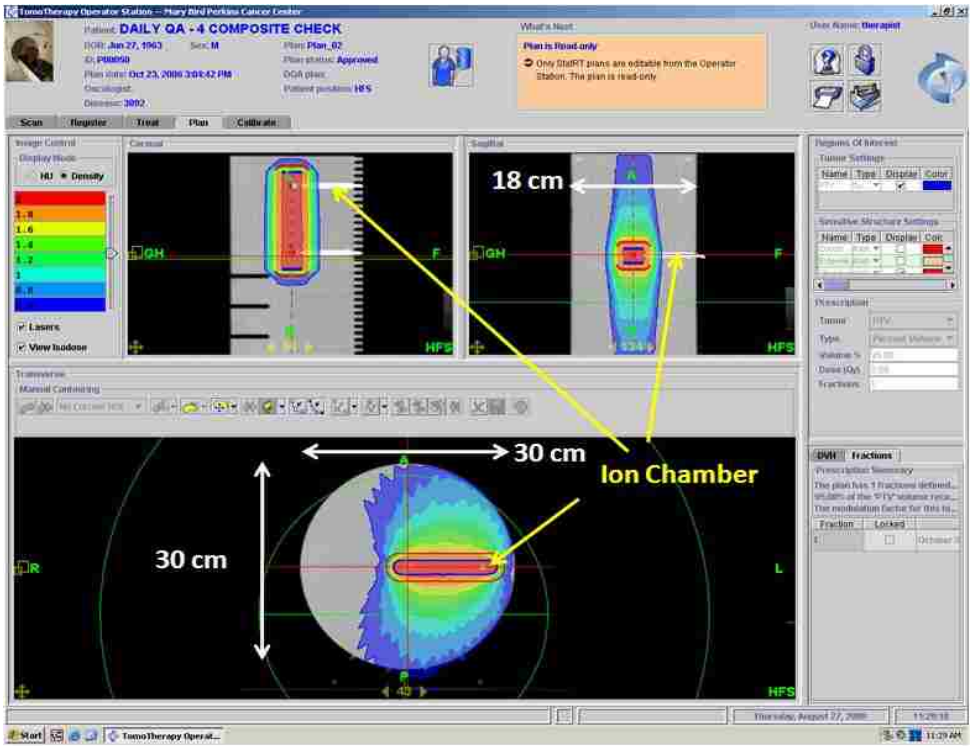

b)

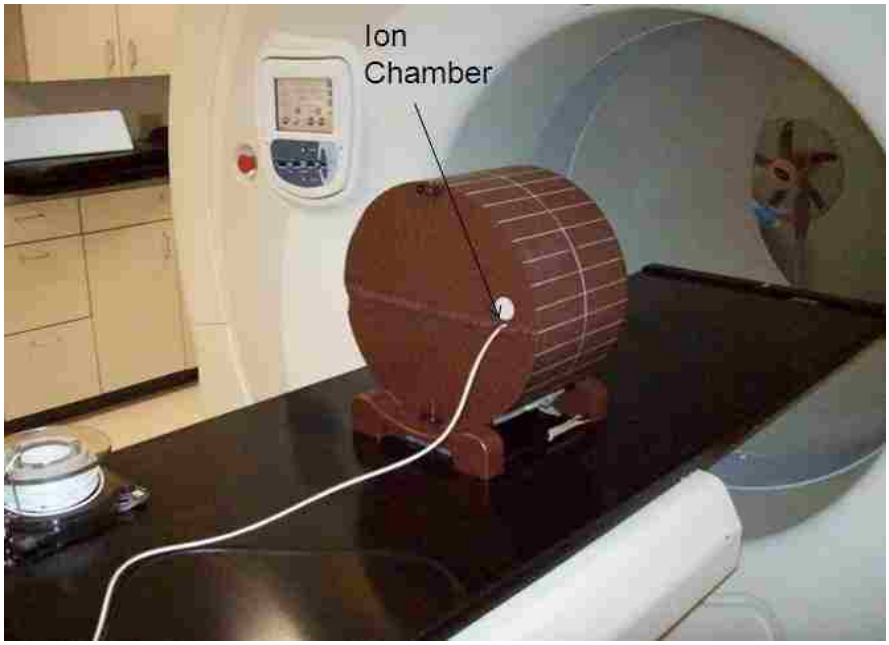

Figure 19. Composite treatment plan a) Screenshot illustrating target volume and isodose distributions for composite QA plan and b) photograph showing Tomo phantom setup before delivery.

where:

D_M = Measured dose (Gy)

M_{raw} = Charge reading from ion chamber

P_{ion} = Correction factor for incomplete ion collection efficiency

P_{TP} = Temperature/pressure correction factor

P_{elec} = Electrometer calibration factor (C/Rdg)

P_{pol} = Polarity correction factor

k_Q = Beam quality conversion factor

$N_{D,W}^{Co_{60}}$ = Ion chamber calibration factor (Gy/C)

At the time of beam commissioning, P_{ion} was found to be 1.004 and P_{pol} was 1.000 determined by MBPCC clinical physicists. Calibration factors for the electrometer and ion chamber have been obtained from an accredited dosimetry calibration laboratory (ADCL) within the last two years. The calibration factor for the electrometer was $P_{elec} = 0.987 \times 10^{-8} \frac{Coulombs}{Reading}$ and $N_{D,W}^{Co_{60}} = 5.446 \times 10^{8} \frac{Gray}{Coulomb}$ for the ion chamber.

Temperature/pressure correction factors were found using the equation:

$$P_{TP} = \frac{273.2+T}{273.2+22.0} \times \frac{101.33}{P}, \quad (19)$$

where:

T = Temperature in °C

P = Pressure in mm of kPa

k_Q is the quality conversion factor which converts the calibration factor for a ^{60}Co beam to that for a beam of quality, Q. It is a function of the photon component of the percent depth dose at 10 cm ($\%dd(10)_x$) under reference conditions (10x10 cm^2 field

size and SSD = 100 cm). Because these reference conditions are impossible to emulate on a TomoTherapy unit, Thomas' method uses $\%dd(10)_x$ for 85 cm SSD and a 5x10 cm^2 field size (64.6%) to find k_Q. k_Q was determined by MBPCC clinical medical physicists at time of commissioning to be 0.996 using the procedure described by Thomas (Thomas, Mackenzie et al. 2005).

Over the course of data collection, the only adjustments other than target change or injector current adjustments was one pulse forming network (PFN) change on October 24, 2008. The PFN determines the input power to the magnetron, controlling the output (TomoTherapy 2008).

The same reduced chi-squares method used in Aim 1 to determine the error was used to find the error in the measured composite dose.

To measure the sensitivity of the composite plan to energy change, the daily measured dose was plotted versus effective energy. This was done for a period of time when no beam adjustments were made (e.g. July 1, 2008 to October 15, 2008 or November 10, 2008 to January 22, 2009). A linear fit was applied to this data set and the slope determined. The slope assumed that the corrected dose was plotted on the y-axis and the effective energy on the x-axis. Using this slope and the known error in measured dose, the sensitivity to energy change in MeV could be determined:

$$S = \frac{\sigma_{Dose}}{m}, \tag{20}$$

where:

S = Sensitivity to energy change (MeV)

m= Slope of effective energy vs. composite dose (MeV^{-1} *Gy)

σ_{Dose} = Error in composite dose (Gy)

Additionally, to test the sensitivity of the composite plan to a known energy change, the data was collected while varying the injector current during a single setup.

Chapter 3. Results and Discussion

I. Aim 1- TQA Software

A. Varying Injector Current

Figure 20 shows the results when the injector current was varied during a single measurement session. The injector current setting ranged from 3.7-3.97 V (the maximum and minimum the system would allow without interlocking) which corresponded to linear attenuation coefficients ranging from 0.1337-0.1368 cm^{-1}. These tests were done sequentially on a single day, April 11, 2009, so that target degradation and machine variation factors would be eliminated. Clearly, as the consistency of the graph shows, there is a linear correlation between the injector current setting and resulting linear attenuation coefficient.

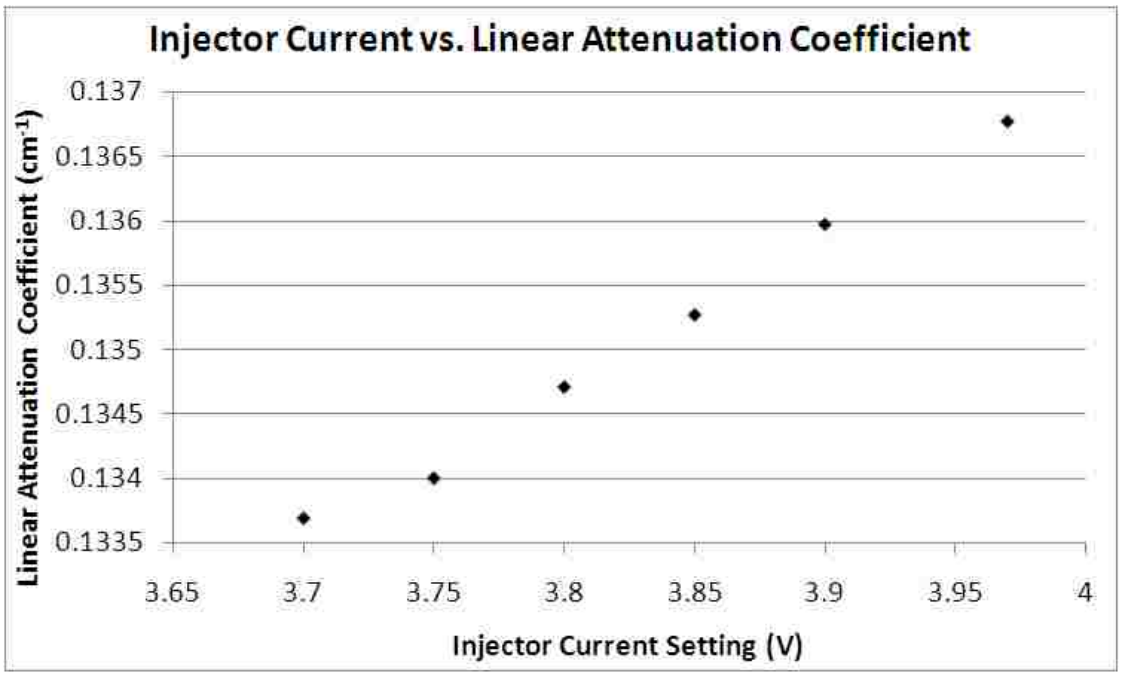

Figure 20. Injector current vs. linear attenuation coefficient.

B. Data Taken Over Lifetime of Target

Data taken using the stepwedge procedure has been plotted over the course of an x-ray target lifetime (June 6, 2008 – January 24, 2009). As mentioned in the methods and materials, the linear attenuation coefficient was calculated for each stepwedge procedure. The data, exported from the TQA software and shown in Figure 21 shows the change in linear attenuation coefficient for all stepwedge runs versus time compared to a user-defined reference. The data show four distinct jumps, indicated by arrows 1-4. Arrow 1 shows the change on June 6, 2008, corresponding to the installation of a new target. Arrow 2 shows the change on June 25, 2008, corresponding to an injector current adjustment. Arrow 3 corresponds to another newly installed target on January 26, 2009. Arrow 4 corresponds to a second injector current adjustment on February 17, 2009. These changes indicate how well the TQA data responds to changes that affect the energy of the beam, such as a target change or the injector current setting adjustment.

Also displayed in the graph are the reference value (μ=0.1312 cm^{-1}) taken on July 14, 2008, and a ±2% window. July 14, 2008 was chosen since it occurred shortly after the target change and immediately after a TQA software update.

Over the lifetime of the target, the linear attenuation coefficient changed approximately 4% (0.130-0.135 cm^{-1}). The consistent trending of the data, other than the four jumps previously discussed, indicates the high sensitivity of the software and stepwedge procedure to a gradual energy change in the beam over time.

As mentioned in the Methods and Materials, the data from Hubbell and Seltzer was used to convert linear attenuation coefficient to photon energy. Figure 21 shows that the linear attenuation coefficient changed only slightly over the time period studied

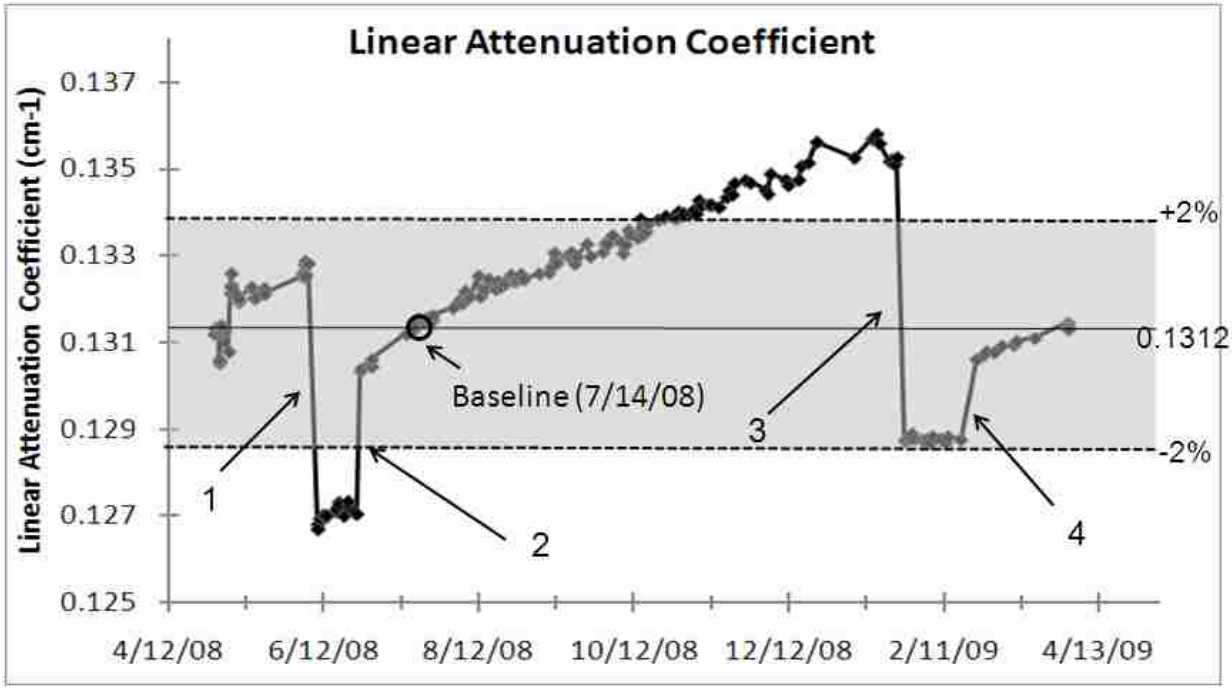

Figure 21. Stepwedge data compared to reference (July 14) over lifetime of target for linear attenuation coefficient with arrows indicating significant changes.

and there are only four values available in the tables spanning this narrow range. Therefore, to interpolate between these table values, a second order polynomial fit of the Hubbell and Seltzer data was used to determine the effective energy at points between table values. This is illustrated in Figure 22 .

The data converted to effective energy are shown in Figure 23. The gray portion represents data within 2% of the reference effective energy, 1.601 MeV. The calculated effective energy changed by about 9% over the lifetime of the target.

To test the error in the stepwedge data, a chi-squared test with a second order least squares polynomial fit was used. The measured values and the corresponding fit for linear attenuation coefficient and effective energy are shown in Figure 24. The

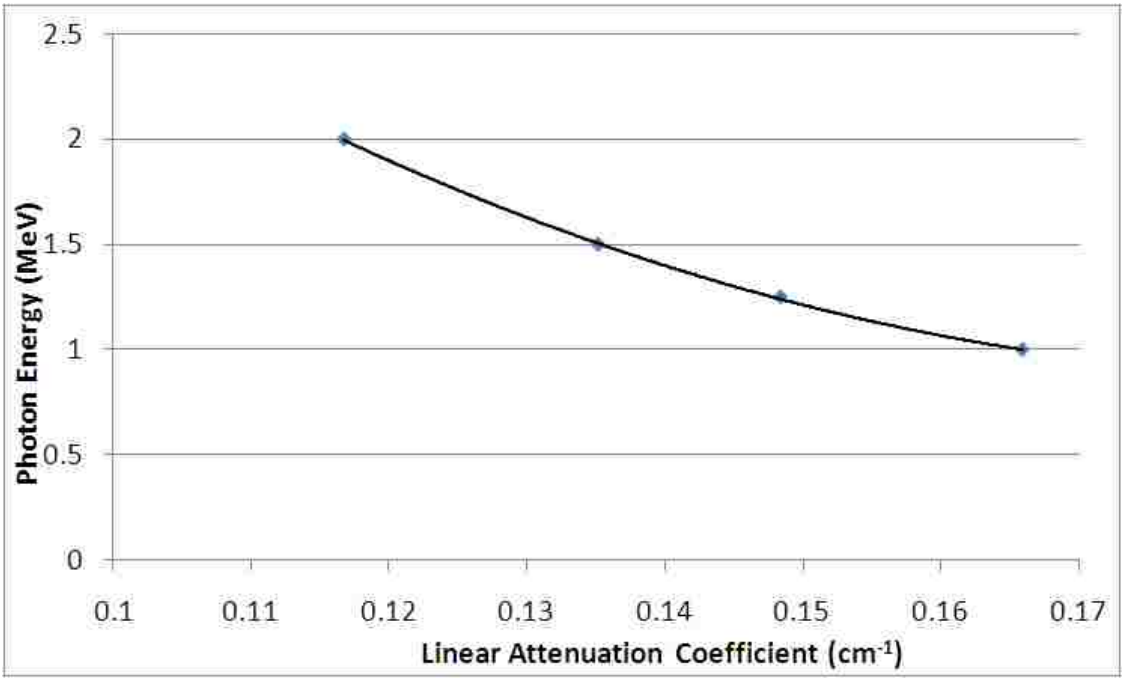

Figure 22. Linear attenuation coefficient and corresponding photon energy for aluminum near values of data collected. Data was interpolated between table values using second-order fit.

individual points represent the measured values and the line through them is the fit data.

The estimated error determined was 1.27×10^{-4} cm^{-1} for the linear attenuation coefficient. After converting the linear attenuation coefficients measured from the software to effective energy, the error in effective energy was then determined by applying a linear fit and using a chi-squared test. The resulting error was found to be 0.0025 MeV for the effective energy. The error for linear attenuation coefficient and effective energy have been added to the data points displayed in Figure 24a and Figure 24b.

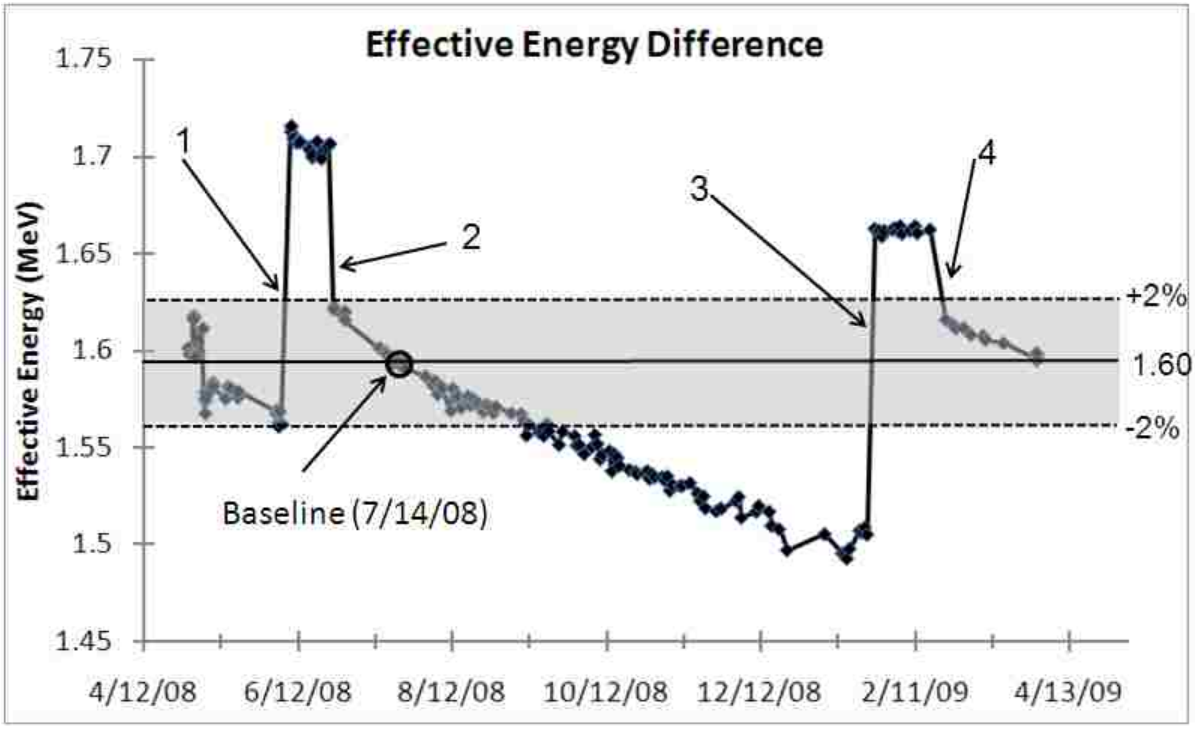

Figure 23. Stepwedge data compared to reference (July 14) over lifetime of target for energy with arrows indicating significant changes.

The resulting sensitivity of 0.0025 MeV corresponds to a 0.16% change in energy as measured using the stepwedge. Hence, a change in effective energy of 2% should be easily detected with this method.

II. Aim 2- Water Tank Setup and Profile Collection

Lateral and PDD profiles were collected in monthly intervals over the lifetime of the target (eight months) using the TEMS system and water tank.

A. Lateral Profiles

The OAR, defined by equation 8, and its associated error (1σ) was plotted versus effective energy, calculated from Aim 1, to determine how sensitive the OAR test was to a change in energy. This was performed for the three commissioned jaw widths; 1, 2.5,

a)

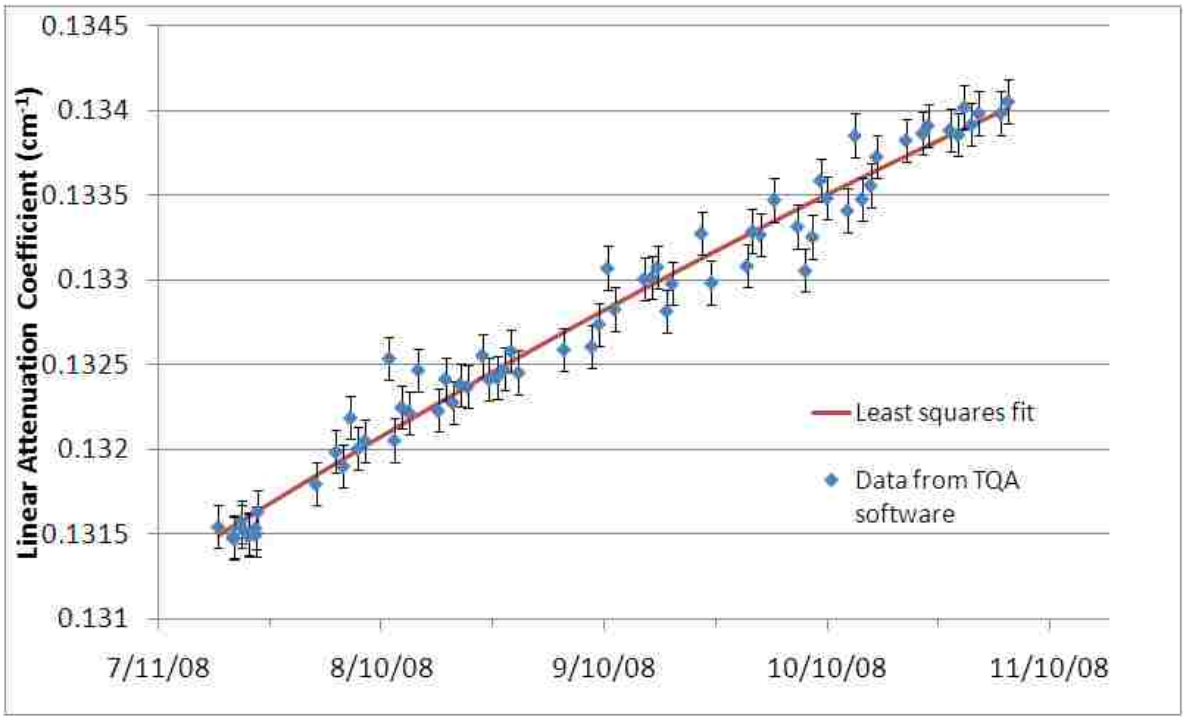

b)

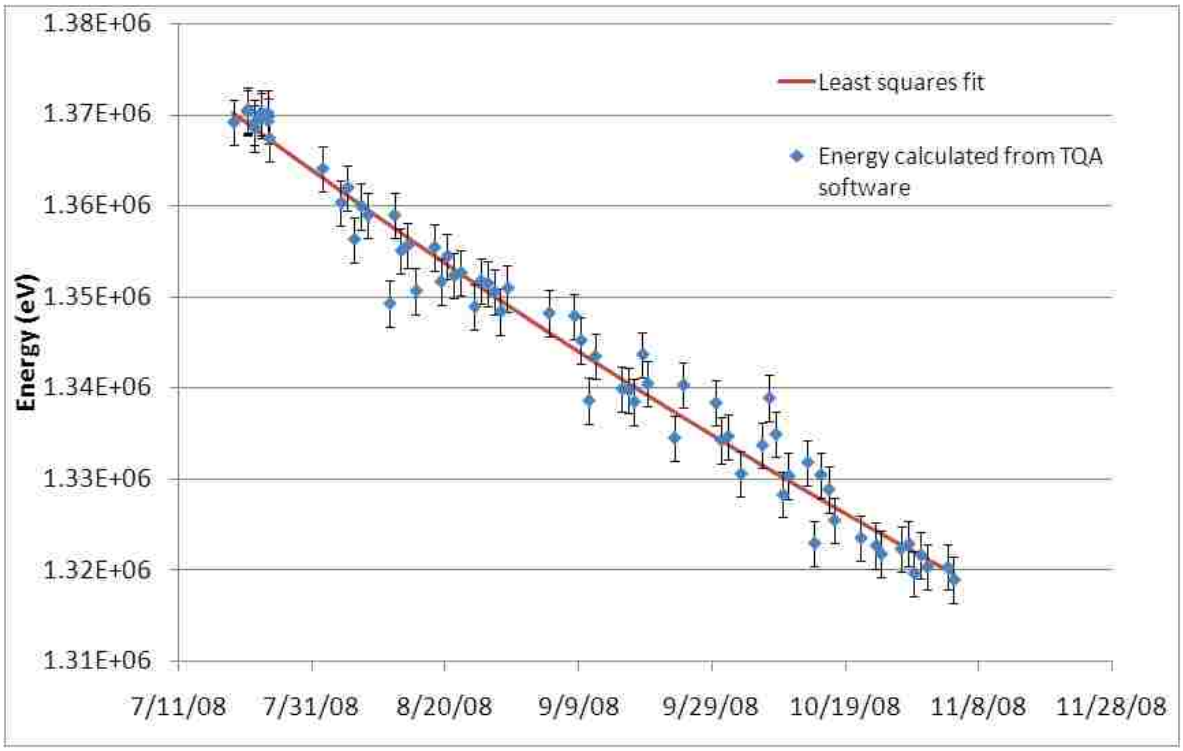

Figure 24. Linear portion of data exported from TQA software for a) linear attenuation coefficient and b) effective energy.

and 5 cm; and at five depths; 1.5, 5, 10, 15, and 20 cm.

i. Varying Injector Current

As was done with the stepwedge setup in Aim 1, the lateral profiles were collected while varying the injector current to test sensitivity to known energy change. The water tank was setup in the same way as when performing monthly scans. Figure 25 shows the lateral profiles for each scan normalized to 100 at the central axis.

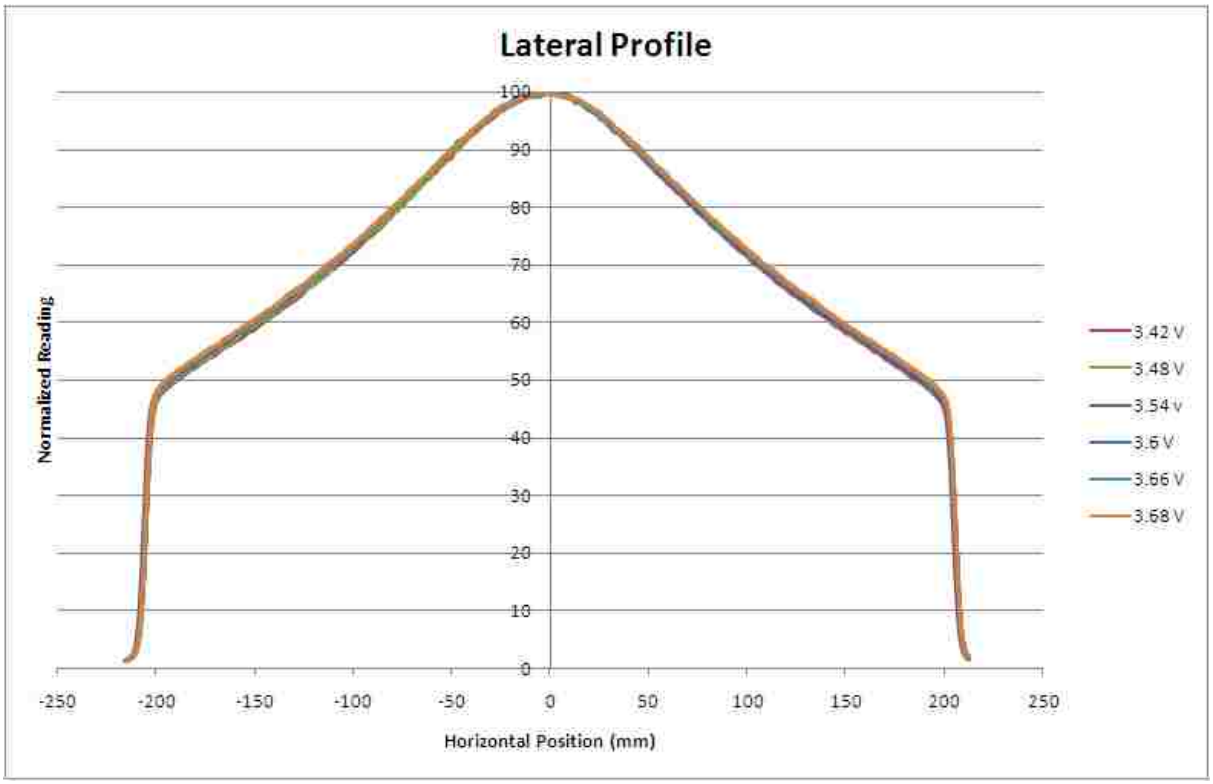

Figure 25. Normalized lateral profiles taken while varying the injector current setting during a single setup.

As was done in Figure 16, the profiles were compared to a reference, the 3.6 V injector current setting, for comparison. This is illustrated in Figure 26. As the injector current was increased, the off-axis ratios were also increased.

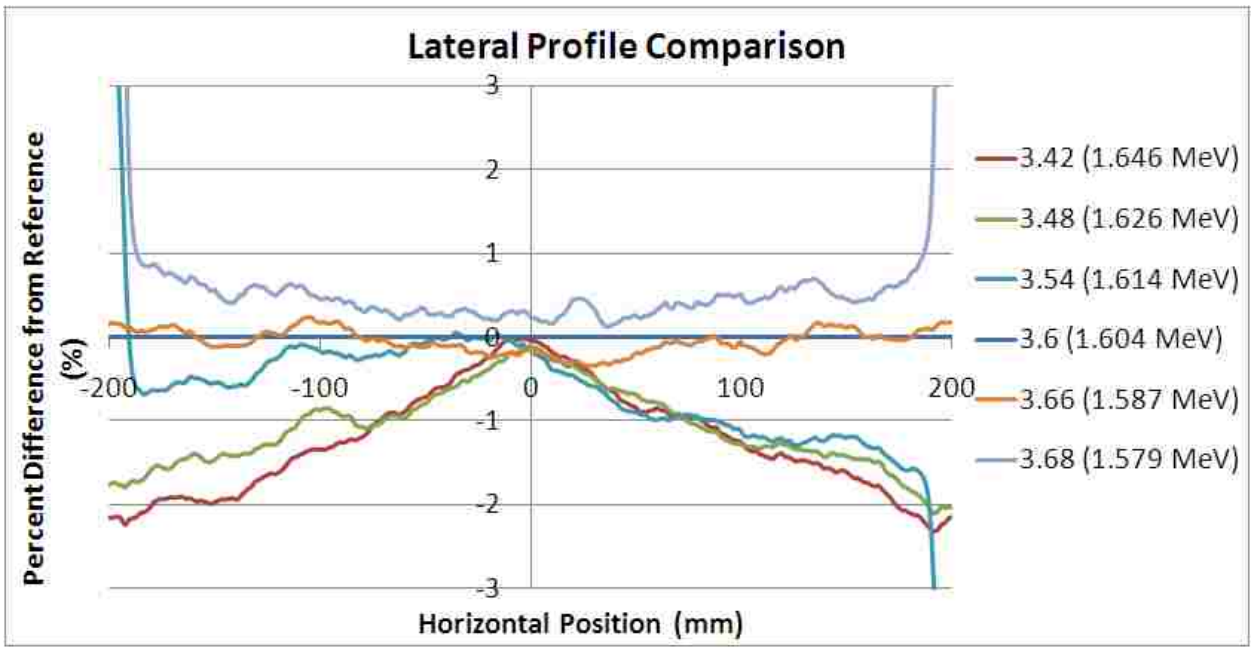

Figure 26. Percent difference from reference (Injector current setting=3.6 V) for lateral profiles taken while varying the injector current setting. All profiles taken at depth=10 cm and nominal jaw width=2.5 cm.

The data were taken using a jaw setting of 2.5 cm and at depths of 1.5, 5, 10, 15, and 20 cm. The effective energy, as determined from Figure 20 and Figure 22, is plotted versus off-axis ratio in Figure 27. One reading was omitted due to its irrelevance to the other data points, shown in red. The data, fit linearly, follows a trend towards lower readings over the lifetime of the target. The data demonstrate a smooth decrease with decreasing energy and is very consistent with the linear fit. Figure 27 shows that collecting lateral profiles and corresponding off-axis ratios is sensitive enough to detect a change in effective energy in a TomoTherapy machine.

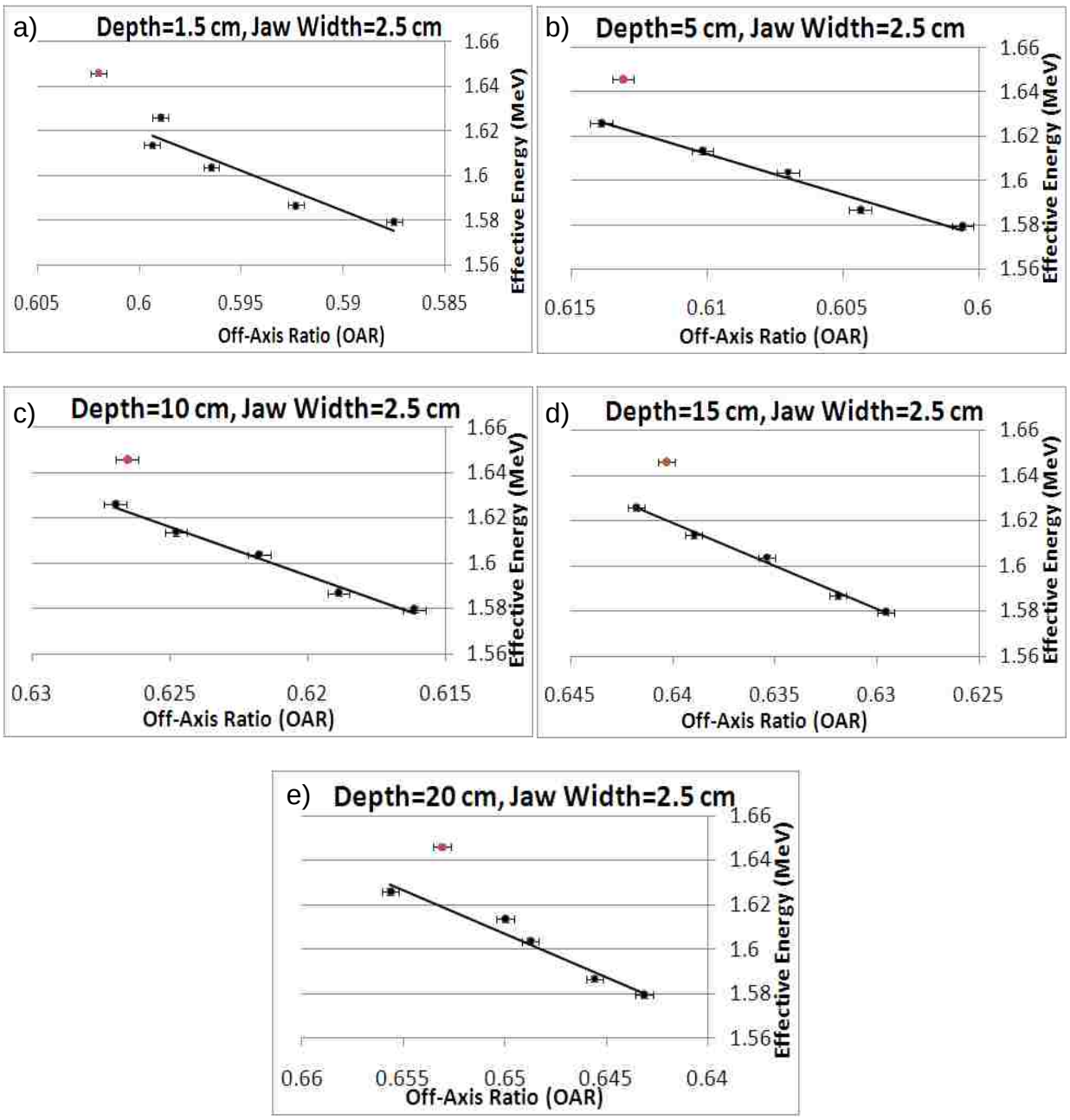

Figure 27. Effective energy vs. OAR for data taken during a single setup while varying the injector current setting using the 2.5 cm jaw width at depths of a) 1.5 cm, b) 5 cm, c) 10 cm, d) 15 cm, and d) 20 cm.

ii. Data Taken Over Lifetime of Target

The plots taken over the lifetime of the target for the three jaw widths and at all five depths are shown in figures 28, 29, and 30. The data were fit linearly and do not demonstrate the consistency with energy change that the data in Figure 27 show.

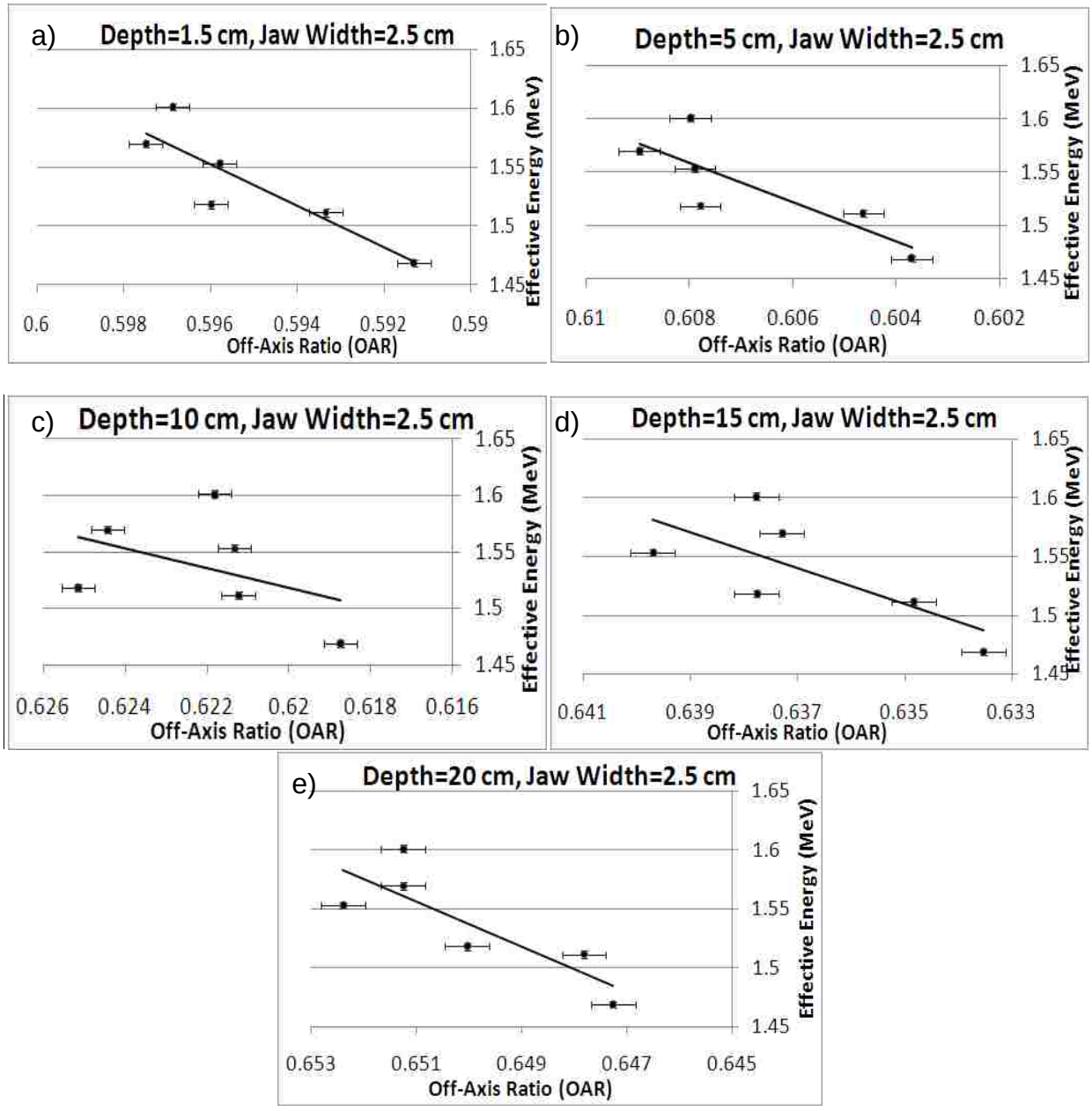

Figure 28**.** Effective energy vs. OAR for data taken over lifetime of target using the 2.5 cm jaw width at depths of a) 1.5 cm, b) 5 cm, c) 10 cm, d) 15 cm, and d) 20 cm.

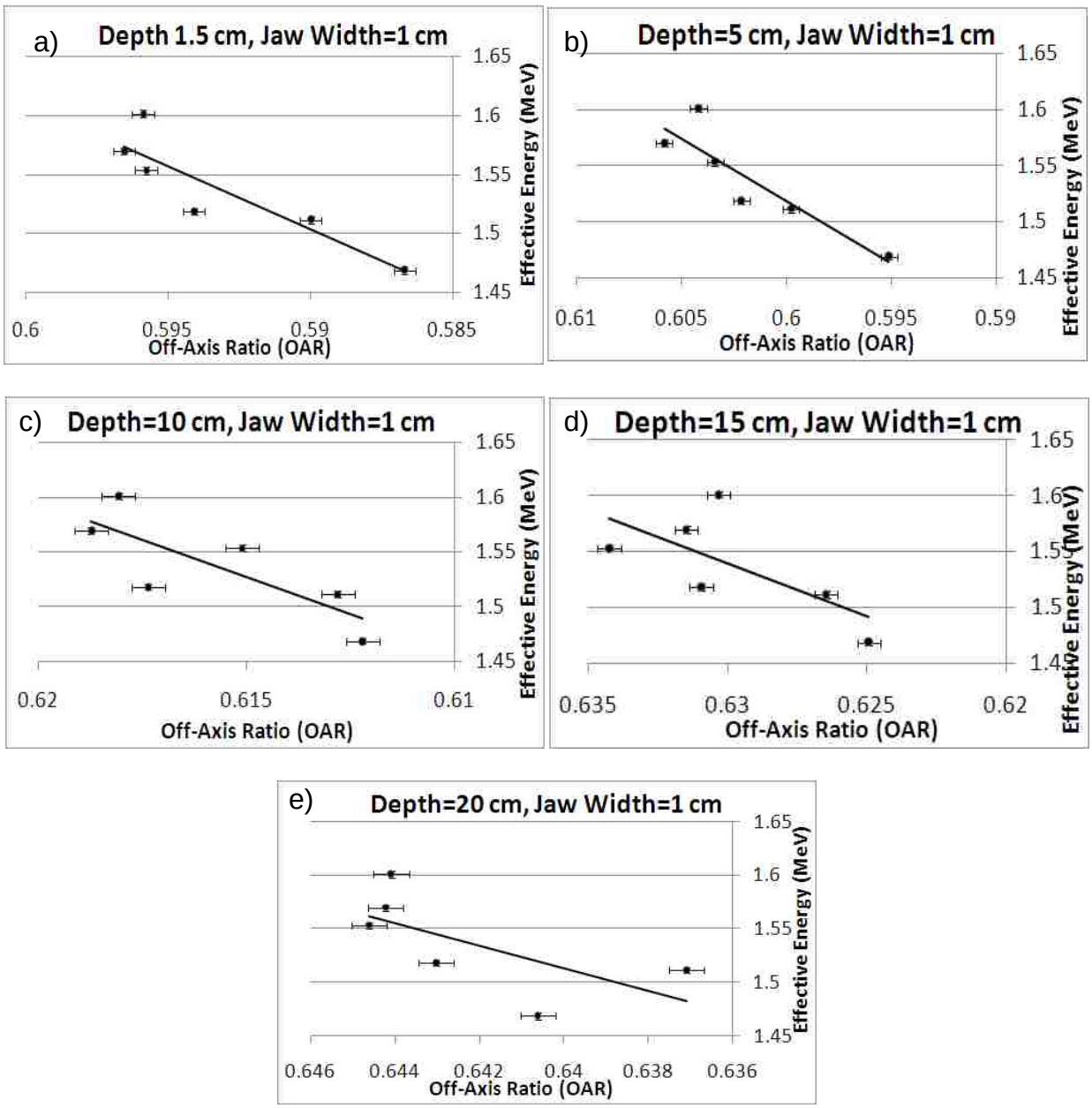

Figure 29. Effective energy vs. OAR for data taken over lifetime of target using the 1 cm jaw width at depths of a) 1.5 cm, b) 5 cm, c) 10 cm, d) 15 cm, and d) 20 cm.

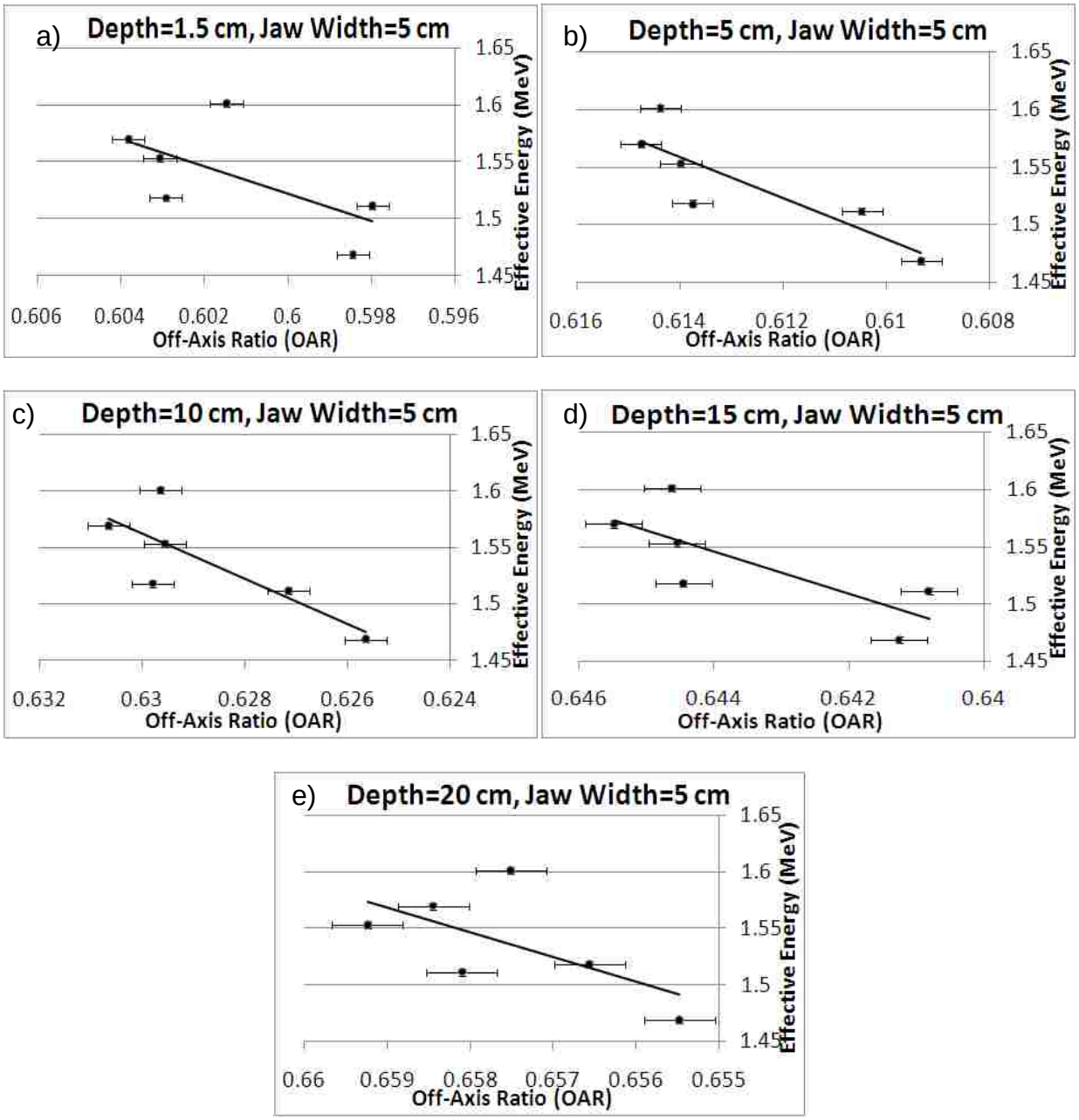

Figure 30**.** Effective energy vs. OAR for data taken over lifetime of target using the 5 cm jaw width at depths of a) 1.5 cm, b) 5 cm, c) 10 cm, d) 15 cm, and d) 20 cm.

Over the lifetime of the target, the off-axis ratios changed by roughly 1-2%. The effective energy over the same period of time changed by about 9%. Over the single setup done while varying the injector current, the off-axis ratio changed by 2-3% while

the effective energy changed by 4%. Even though the single setup energy variation was smaller, the off-axis ratio changed by a larger amount.

Table 3. OAR sensitivity test to energy change.

Off-Axis Ratios	σ_{OAR}=.0007				
Jaw Width (cm)	Depth (cm)	Slope (MeV^{-1})	r^2	Sensitivity (MeV)	Avg. Sensitivity (MeV)
1	1.5	0.075±.0036	0.796	0.009	0.013
	5	0.073±.0037	0.81	0.010	
	10	0.047±.0038	0.64	0.015	
	15	0.049±.0038	0.472	0.014	
	20	0.041±.0040	0.426	0.018	
2.5	1.5	0.044±.0037	0.784	0.016	0.019
	5	0.037±.0037	0.681	0.019	
	10*				
	15	0.034±.0039	0.52	0.021	
	20	0.036±.0040	0.69	0.019	
5	1.5*				
	5	0.042±.0038	0.739	0.017	0.020
	10	0.033±.0039	0.658	0.021	
	15	0.032±.0040	0.593	0.022	
	20*				
2.5 (Varying Inj. Curr.)	1.5	0.202±.0070	0.879	0.003	0.004
	5	0.197±.0071	0.977	0.004	
	10	0.166±.0073	0.987	0.004	
	15	0.181±.0075	0.994	0.004	
	20	0.169±.0076	0.955	0.004	

Table 3 displays the resulting sensitivity test to energy change using the slopes of the linear fits through OAR data plotted versus effective energy. The r^2 values for each depth and jaw width are shown along with the error in the OAR. The r^2 values taken over the lifetime of the target are not as high as those taken while varying the injector current and indicate less of a correlation to the data. The error in the measurement divided by the slope in MeV produced the sensitivity. A few measurements (jaw width=2.5 cm, depth=10 cm; jaw width=5 cm, depth=1.5, 20 cm) indicated by the asterisk in the table were omitted as the data was deemed too inconsistent to model using a linear fit. To better generalize each jaw width with a single value, the average of the sensitivities were calculated and displayed. Clearly, the

data taken while varying the injector current produces a more sensitive test to energy change than that taken over the lifetime of the target. The sensitivity in MeV could be associated with a percent change in energy. Over the lifetime of the target, the average sensitivity was about 0.017 MeV, which corresponded to a 1.1% change in energy. For the data taken while varying the injector current, the sensitivity was about 0.004 MeV, or 0.24%.

B. Percent Depth Dose (PDD) Profiles

PDD, which plots the normalized reading (fraction of maximum dose) versus depth in water profiles, were analyzed similar to lateral profiles and OAR.

i. Varying Injector Current

The data collected while varying the injector current are shown in Figure 31. Again, this was only done for the 2.5 cm jaw setting.

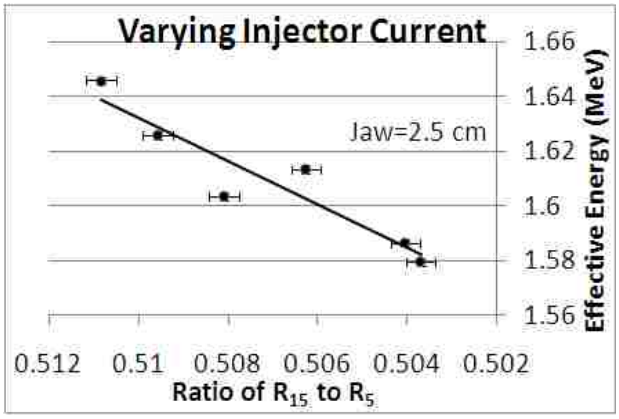

Figure 31. Effective energy vs. ratio of ionization reading at 15-cm depth to reading at 5-cm depth in water from PDD profile for data taken while varying the injector current setting during a single setup.

ii. Data Taken Over Lifetime of Target

Figure 32 illustrates the relationship between the ratios and the corresponding effective energy measured using the aluminum stepwedge for that day. The figure shows the data collected from all three jaw widths.

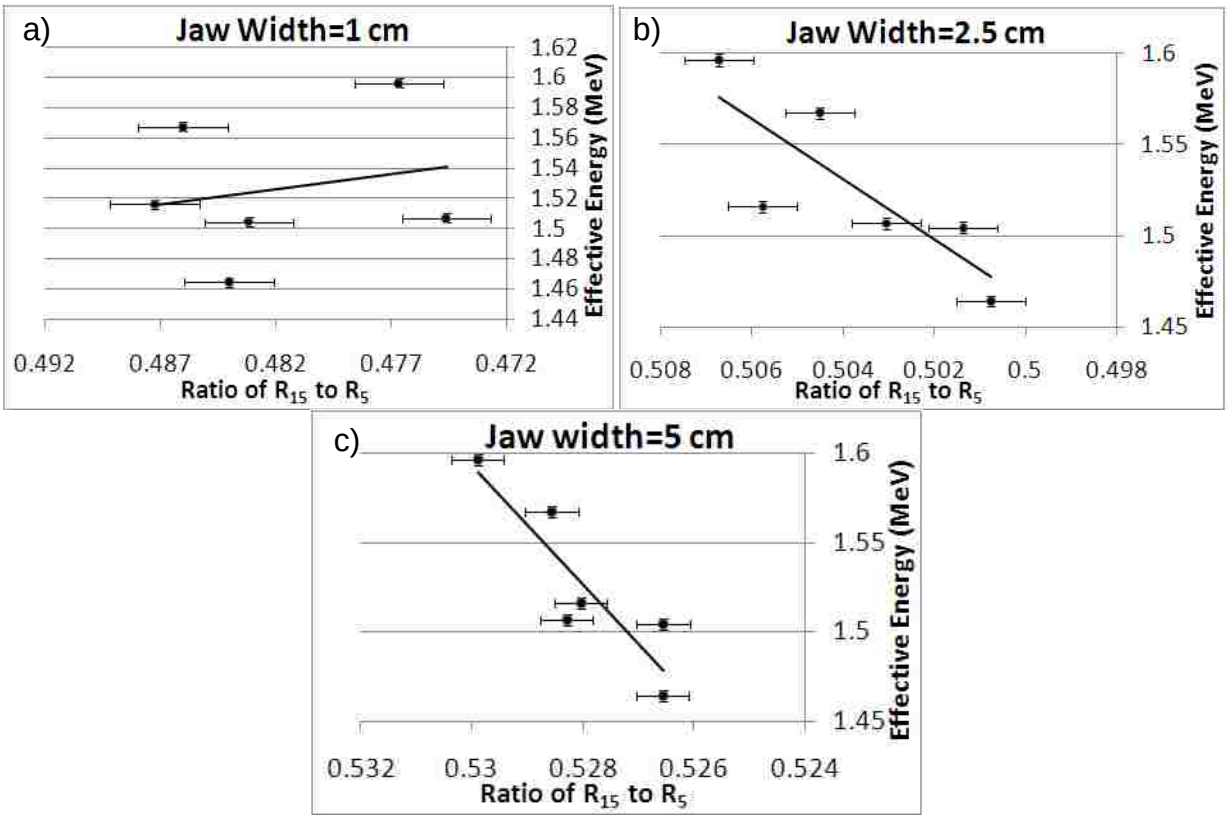

Figure 32. Effective energy vs. ratio of ionization reading at 15-cm depth to reading at 5-cm depth in water from PDD profile for a) 1 cm, b) 2.5 cm, and c) 5 cm jaw widths.

The graphs of PDD ratio versus effective energy were fit linearly to determine the slope and then the sensitivity to energy change.

Table 4 shows the sensitivity of the PDD ratios to energy change. The 1 cm jaw width was omitted due to its lack of any correlation to a linear fit. The average

sensitivity of the data taken over the lifetime of the target was 0.019 MeV, or 1.2%. The sensitivity of the data taken while varying the injector current was 0.003 MeV, or 0.18%.

Table 4. PDD ratio sensitivity test to energy change.

PDD Ratios					
Jaw Width (cm)	Slope (MeV^{-1})	$\sigma_{Ratio15/5}$	r^2	Sensitivity (MeV)	Average Sensitivity (MeV)
1*					
2.5	0.041±.007	0.0008	0.678	0.018	0.019
5	0.024±.007	0.0005	0.787	0.020	
2.5 (Varying Inj. Curr.)	0.111±.014	0.0003	0.881	0.003	0.003

III. Aim 3-Composite Plan

Recorded for each daily run of the Daily QA-4 Composite Plan procedure was the delivered number of cumulative monitor units, the temperature and pressure, and the reading on the electrometer, M_{raw}. The recorded temperature and pressure were used in determining P_{TP} as shown in the Methods and Materials. Using these data, the measured dose can be calculated for each day as shown in the Methods and Materials. To account for any day to day variations in machine output, the measured dose was scaled to the value had the expected number of monitor units been delivered, i.e.:

$$Corrected\ Composite\ Dose\ (Gy) = D_M\ x\ \frac{MU_{exp}}{MU_{del}}, \quad (21)$$

where:

D_M = Measured dose (Gy)

MU_{exp} = Expected number of monitor units (2329)

MU_{del} = Delivered number of monitor units

A. Varying Injector Current

To test how sensitive the composite dose results were to manual changes in energy, similar to what was done in the first two aims, a change in the injector current setting

was made during a single setup and the composite dose plan was run. The results, shown in Figure 33, indicate a direct relationship between injector current setting and resulting measured dose. Therefore, the composite plan would be capable of detecting an energy change.

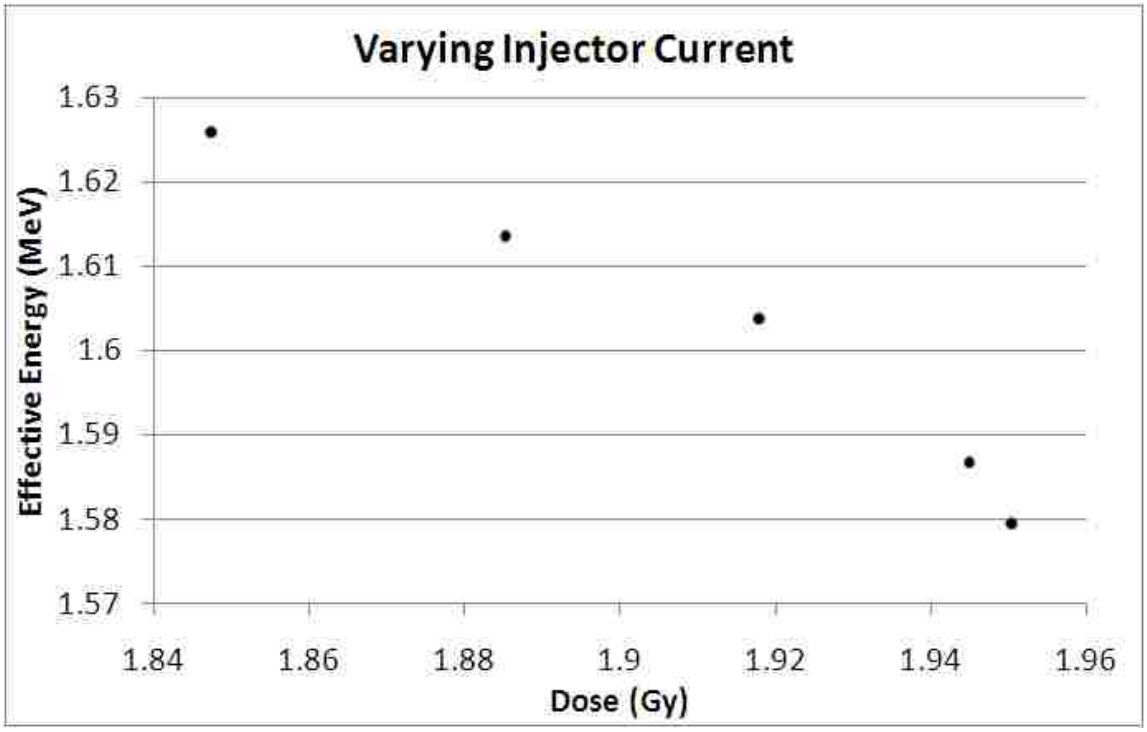

Figure 33. Composite dose values measured while varying the effective energy.

B. Data Taken Over Lifetime of Target

Results over the 8 month period of data acquisition for the normalized composite doses are shown in Figure 34.

Arrows 1 and 4 indicate target changes and arrows 2 and 5 indicate injector current adjustments. Arrow 3 indicates the PFN adjustment. Other than a few aberrations, the data stay within 2% over the length of the x-ray target. Also, there seems to be a trend towards lower dose values over time with the exception of arrow 3.

As was done for Aim 1, a second-order least squares fit was used to fit a portion of the data. The dates used were from July 2, 2008 to September 15, 2008.

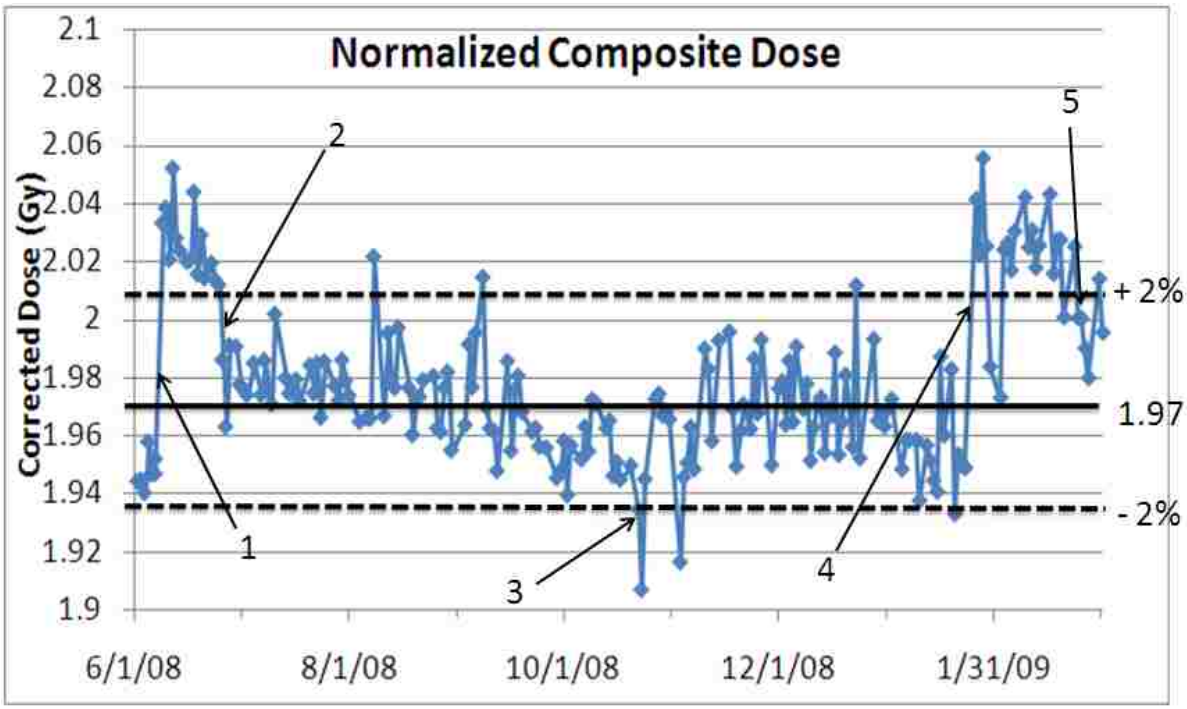

Figure 34. Normalized Composite dose over lifetime of x-ray target. Expected dose of 1.97 is indicated by solid black line with ±2% by the dotted lines.

Using the χ^2 method described in Aim 1, σ was determined to be 0.013 gray. To test the sensitivity of the composite plan to energy, the composite doses for each day over the same time period as shown in Figure 35 were plotted versus the effective energy for that day. A linear fit was applied to this data and the slope was determined. A few of the dose points, those outside of two gray, were omitted. This is shown in Figure 36.

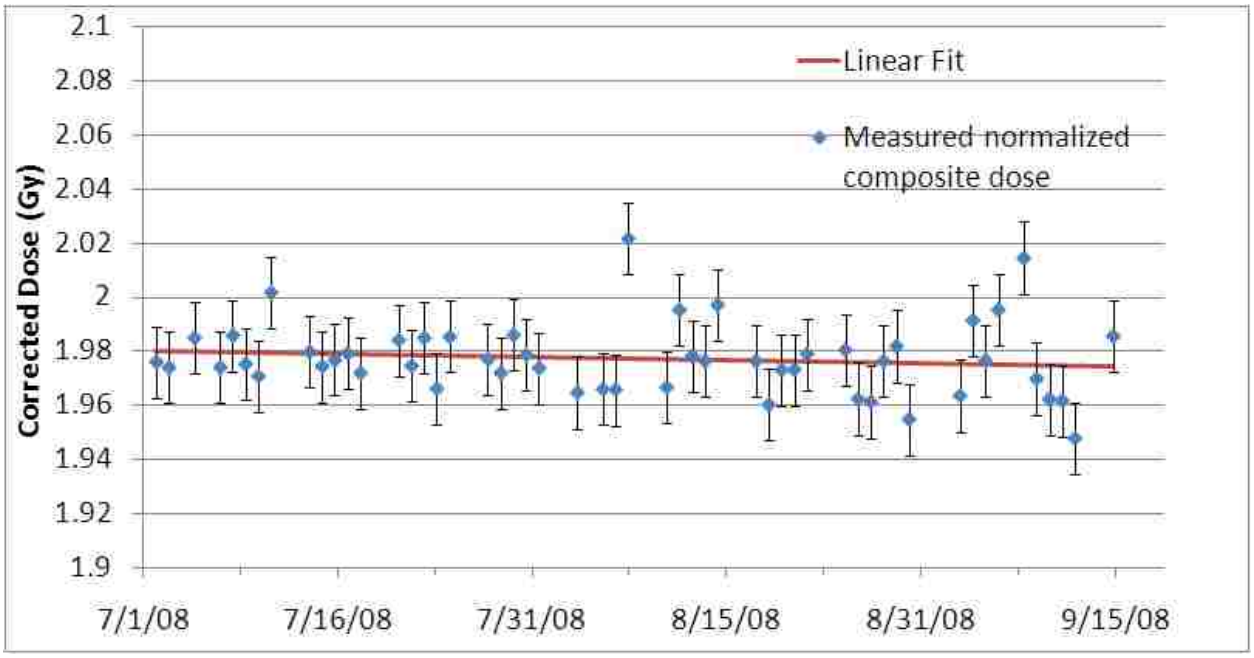

Figure 35. Linear portion of normalized composite dose data fit using a straight line.

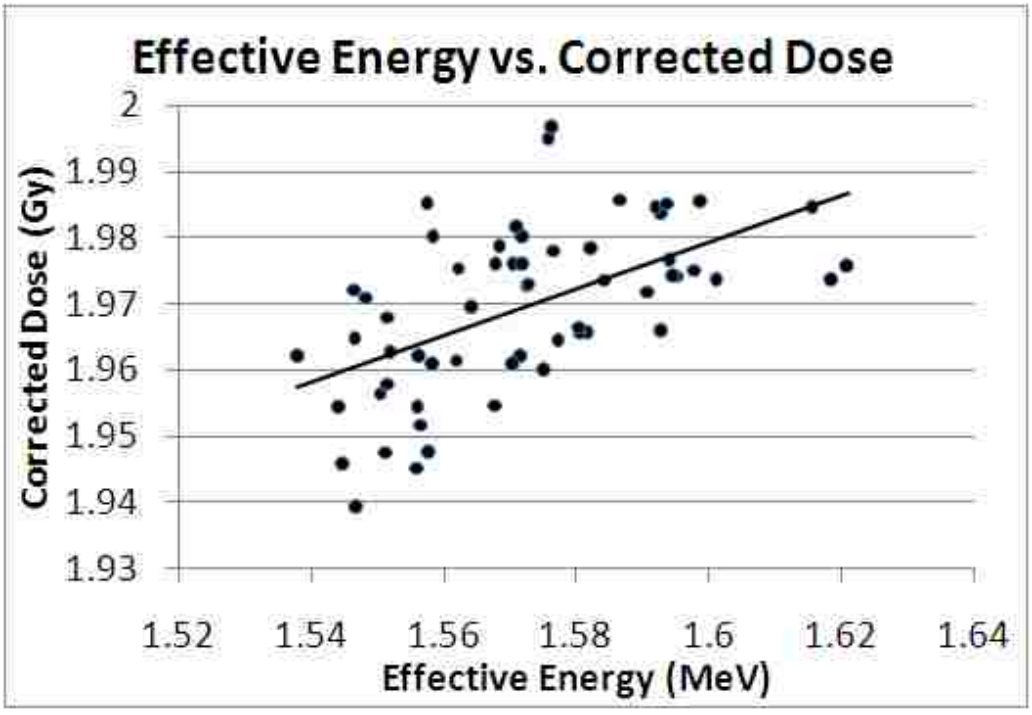

Figure 36. Effective energy vs corrected dose from composite IMRT plan. A linear fit is applied to the data points to determine the slope.

The resulting sensitivity of the composite plan is shown in Table 5.

Table 5. Composite plan sensitivity test to energy change.

Composite Plan			
Slope (Gy/MeV)	σ_{Dose} (Gy)	r^2	Sensitivity (MeV)
0.354	0.013	0.19	0.037

The r^2 value associated with the composite plan is much less than that for the previous aims and must be kept in mind during analysis. The sensitivity to energy change was 0.037 MeV, or 2.3%.

As the hypothesis stated, an energy change of 2% could be detected using the three aims. A summary of the three aims and their associated ability to detect a change in energy is shown below in Table 6.

Table 6. Summary of sensitivities of the three aims.

			Sensitivity (MeV)	% Change in Energy
Aim 1	Stepwedge		0.0025	0.16
Aim 2	Off-Axis Ratios			
		Varying Injector Current	0.004	0.24
		Lifetime of Target	0.017	1.08
	PDD Ratios			
		Varying Injector Current	0.003	0.18
		Lifetime of Target	0.019	1.19
Aim 3	Composite Dose		0.037	2.30

The only data taken that was outside of the 2% requirement was the composite dose data. However, the data over the lifetime of the target is not nearly as accurate as the data from the stepwedge or that taken while varying the injector current.

Chapter 4. Conclusions and Recommendations

I. Conclusions

The hypothesis of this study stated that an effective energy change of 2% could be detected using either attenuation data acquired with an aluminum stepwedge, or water phantom scans of lateral or depth dose profiles. This hypothesis was tested using three aims: Aim 1, obtain exit detector data daily over lifetime of x-ray target for a) a rotational procedure using an unattenuated beam and b) a topographic procedure using an aluminum stepwedge; Aim 2, collect lateral and percent depth dose (PDD) profiles monthly, and Aim 3, obtain composite dose data collected from Daily QA plans run each day during machine warmup over lifetime of target.

In aim 1, exit detector data was gathered over the lifetime of an x-ray target as well as during a single setup while varying the injector current in order to monitor the change in linear attenuation coefficient and effective energy. The percent difference of measured linear attenuation coefficients over time compared to a reference, collected using TQA software, increased linearly over time. This corresponded to a decrease in the effective energy of the beam. The software detected a 9% change in effective energy over the lifetime of the target with each reading accurate to 0.2%. A sensitivity test showed that using the stepwedge a change in energy of 0.0025 MeV could be detected. This corresponded to a 0.2% change in energy, easily meeting the hypothesis of detecting a 2% change.

In aim 2, lateral and percent depth dose (PDD) scans were taken on a monthly basis using a water tank scanning system specific to TomoTherapy. Also, to determine how sensitive the profiles were to a change in energy without a degraded target, scans were done on a single day by varying the injector current setting. Average off-axis

ratios for each lateral profile collected were calculated. The ratios were plotted versus effective energy to determine the sensitivity of off-axis ratio to energy change. For the data taken over the lifetime of the target, the sensitivity to energy change was found to be 0.011 MeV or 0.7%. From the data taken while varying the injector current, the sensitivity to energy change for OAR was found to be 0.003 MeV, or 0.2%. Collecting lateral profiles seems to be easily sensitive enough to detect an energy change of 2%. The same analysis was done for PDD profiles, using the ratio of the reading at 15 cm to 5 cm in the place of OAR. The process was also done for the setup while varying the injector current. Over the lifetime of the target, the sensitivity to energy change was found to be 0.041 MeV, or a 2.7%. For the single scan while varying the injector current, the sensitivity to energy change was 0.005 MeV, or 0.3%. These values indicate that PDD ratios were not as sensitive as off-axis ratios and over the lifetime of the target were not sensitive enough to detect a 2% change in energy.

In aim 3, doses calculated from a composite IMRT plan collected daily during machine warmup were analyzed over the lifetime of the x-ray target. The doses were plotted versus effective energy to determine the sensitivity of the measurement to energy change. It was shown that a 0.011 MeV, or 0.7%, change in energy could be detected using the composite plan. This method seems to be sensitive enough to detect a 2% change in energy, although the relative r^2 value takes away some of the significance.

Although the resulting sensitivity test to energy change for each aim showed that a 2% change could be detected (with the exception of the PDD ratios over the lifetime of the target), the most sensitive methods were that of the stepwedge and the water scan data taken while varying the injector current for a single scan. The errors associated

with the water scan data were higher than those associated with the stepwedge data. Also, the fit for the stepwedge data was much more accurate than that for the off-axis ratios and PDD ratios.

II. Clinical Impact and Recommendations

The TQA software is easily implemented into the clinic and can be interfaced with the machine with a simple wire connection. The setup is quick and easily learned and the processing of the data straightforward. Due to the small amount of time required for setup, delivery, and analysis compared to the large amount and high sensitivity, especially for effective energy, of data gathered, implementation of the software is recommended for clinics with a TomoTherapy unit. The water tank scans and composite dose plans are suitable for ensuring the machine is performing within tolerances or detecting an energy change over a short period of time. However, their lack of sensitivity to energy change accompanying a degrading target make the stepwedge procedure with the TQA software preferable

References

Almond, P. R., P. J. Biggs, et al. (1999). "AAPM's TG-51 protocol for clinical reference dosimetry of high-energy photon and electron beams." Med Phys **26**(9): 1847-70.

Bevington, P. R. and D. K. Robinson (1992). Data Reduction and Error Analysis for the Physical Sciences, McGraw Hill.

Bortfeld, T. R., D. L. Kahler, et al. (1994). "X-ray field compensation with multileaf collimators." Int J Radiat Oncol Biol Phys **28**(3): 723-30.

Chang, S. X., T. J. Cullip, et al. (2004). "Compensators: an alternative IMRT delivery technique." J Appl Clin Med Phys **5**(3): 15-36.

Dyk, J. V. (2005). The Modern Technology of Radiation Oncology. Madison, Medial Physics Publishing.

Fenwick, J. D., W. A. Tome, et al. (2004). "Quality assurance of a helical tomotherapy machine." Phys Med Biol **49**(13): 2933-53.

Graf, R., P. Wust, et al. (2009). "Potentials of on-line repositioning based on implanted fiducial markers and electronic portal imaging in prostate cancer radiotherapy." Radiat Oncol **4**: 13.

Grant, W. (1999). Intensity Modulated Radiation Therapy with the Peacock System. A Practical Guide to 3-D Planning and Conformal Radiation Therapy. J. A. Purdy and G. Starkschall. Middleton, WI, Advanced Medical Publishing, Inc.

Greene, D. (1986). Linear Accelerators for Radiation Therapy. Accord, Adam Hilger.

Hubbell, J. H. and S. M. Seltzer. (2004). "Tables of X-Ray Mass Attenuation Coefficients and Mass Energy-Absorption Coefficients."

Kapatoes, J. M., G. H. Olivera, et al. (2001). "A feasible method for clinical delivery verification and dose reconstruction in tomotherapy." Med Phys **28**(4): 528-42.

Karzmark, C. J., C. S. Nunan, et al. (1993). Medical Electron Accelerators. New York, McGraw Hill, Inc-Health Professions Divisions.

Keller, H., M. Glass, et al. (2002). "Monte Carlo study of a highly efficient gas ionization detector for megavoltage imaging and image-guided radiotherapy." Med Phys **29**(2): 165-75.

Khan, F. M. (2003). The Physics of Radiation Therapy, Lippincott Williams and Wilkins.

Kutcher, G. J., L. Coia, et al. (1994). "Comprehensive QA for radiation oncology: report of AAPM Radiation Therapy Committee Task Group 40." Med Phys **21**(4): 581-618.

Langen, K. M., S. L. Meeks, et al. (2005). "Evaluation of a diode array for QA measurements on a helical tomotherapy unit." Med Phys **32**(11): 3424-30.

LoSasso, T., C. S. Chui, et al. (1998). "Physical and dosimetric aspects of a multileaf collimation system used in the dynamic mode for implementing intensity modulated radiotherapy." Med Phys **25**(10): 1919-27.

Low, D. A., S. Mutic, et al. (1999). "Abutment region dosimetry for serial tomotherapy." Int J Radiat Oncol Biol Phys **45**(1): 193-203.

Mackie, T. R. and J. Balog (1999). "Tomotherapy." Seminars in Radiation Oncology **9**(1): 108-117.

Mackie, T. R., T. Holmes, et al. (1993). "Tomotherapy: a new concept for the delivery of dynamic conformal radiotherapy." Med Phys **20**(6): 1709-19.

Mackie, T. R. and G. H. Olivera (2003). "Helical Tomotherapy." 247-281.

Otto, K. (2008). "Volumetric modulated arc therapy: IMRT in a single gantry arc." Med Phys **35**(1): 310-7.

Purdy, J. A. (2001). "Intensity-modulated radiotherapy: current status and issues of interest." Int J Radiat Oncol Biol Phys **51**(4): 880-914.

Purdy, J. A. and G. Starkschall (1999). A Practical Guide to 3-D Planning and Conformal Radiation Therapy. Madison, Advanced Medical Publishing, Inc.

Siochi, R. A. (1999). "Minimizing static intensity modulation delivery time using an intensity solid paradigm." Int J Radiat Oncol Biol Phys **43**(3): 671-80.

Staton, R. J., K. M. Langen, et al. (2009). "Dosimetric effects of rotational output variation and x-ray target degradation on helical tomotherapy plans." Med Phys **36**(7): 2881-2888.

Thomas, S. D., M. Mackenzie, et al. (2005). "A Monte Carlo derived TG-51 equivalent calibration for helical tomotherapy." Med Phys **32**(5): 1346-53.

TomoTherapy (2007). TomoTherapy HI-ART User Guide.

Tomotherapy. (2008). from http://www.jolietoncology.com/tomotherapy.html.

TomoTherapy (2008). Tomo QA Guide.

Yu, C. (1997). Intensity Modulated Arc Therapy: A new method for delivering conformal radiation therapy. Madison.

Vita

Todd Racine was born in Indianapolis, Indiana in September of 1983, the son of Randy and Nancy Racine. After graduating from Noblesville High School in 2002, he enrolled at Ball State University in Muncie, Indiana. In May of 2006, he received his bachelor's degree in physics. He enrolled in Louisiana State University's medical physics program in the fall of 2006.